DEPARTMENT OF INTERNATIONAL AND EUROPEAN ECONOMIC STUDIES

ATHENS UNIVERSITY OF ECONOMICS AND BUSINESS

Assessing the impact of climate change on mean annual wave agitation and berth downtime at two major ports of the Eastern Mediterranean Sea: Port of Piraeus, Greece and Port of Limassol, Cyprus

Michalis Chondros
Andreas Papadimitriou
Anastasios Metallinos
Vasiliki Chalastani
Conrad Landis
Dimitris Spyrou
Chrysi Laspidou
Phoebe Koundouri
Vasiliki Tsoukala

Working Paper Series

25-51

August 2025

Assessing the impact of climate change on mean annual wave agitation and berth downtime at two major ports of the eastern Mediterranean Sea: Port of Piraeus, Greece and Port of Limassol, Cyprus

Michalis Chondros[a], Andreas Papadimitriou[a], Anastasios Metallinos[a], Vasiliki Chalastani[a], Conrad Landis[d], Dimitris Spyrou[b], Chrysi Laspidou[c], Phoebe Koundouri[d] and Vasiliki Tsoukala[a,*]

[a] Laboratory of Harbour Works, School of Civil Engineering, National Technical University of Athens, Zografou, 15780, Greece

[b] Piraeus Port Authority S.A., Marketing & Quality Control department, EU co-funded projects, 18538, Piraeus, Greece

[c] Civil Engineering Department, University of Thessaly, Pedion Areos, Volos 38334, Greece

[d] School of Economics and ReSEES Research Laboratory, Athens University of Economics and Business; Department of Earth Sciences, University of Cambridge;
Sustainable Development Unit, ATHENA RC; Academia Europea

[*] Corresponding author. *E-mail address*: tsoukala@mail.ntua.gr

Abstract

This study assesses the impact of climate change on mean annual wave agitation and berth downtime at two major Eastern Mediterranean ports: the Port of Piraeus, Greece, and the Port of Limassol, Cyprus. Using high-fidelity numerical modeling under two climate scenarios (RCP4.5 and RCP8.5) up to 2100, changes in wave agitation within the port basins are evaluated, both with and without accounting for Sea Level Rise (SLR). Results indicate that climate change will not lead to a uniform increase in wave agitation; rather, outcomes vary depending on the adopted RCP scenario, time period, and specific location within each port basin. While SLR does not significantly alter mean annual wave agitation, its contribution is evident as a slight increase in agitation compared to scenarios excluding SLR. Regarding mean annual berth downtime, more exposed berths in both ports are projected to face significant increases. The influence of SLR on downtime is inconsistent, especially at the Port of Piraeus, where it may increase, decrease, or have negligible effects depending on location. These findings highlight the complex interplay between wave dynamics, local geomorphology, and port infrastructure, emphasizing the importance of port-specific climate resilience assessments.

Keywords: wave agitation, numerical modelling, climate change, sea level rise, port basin, berth down time, port operability

Highlights:

- Comprehensive analysis of future wave climate and Sea Level Rise (SLR) impacts on wave agitation within the Ports of Piraeus and Limassol under RCP4.5 and RCP8.5 scenarios.
- No consistent increase in mean annual wave agitation is observed across both port basins; results vary based on the RCP scenario, time horizon, and specific basin location.
- SLR slightly amplifies wave agitation within the basins but has a variable impact on berth downtime, which depends on the berth's location.
- The more exposed berthing positions are projected to experience significant increases in downtime.

1 Introduction

Ports are critically important infrastructure for global trade, economic growth and regional development (IMO, 2012; UNCTAD 2021). They serve as essential hubs that facilitate the movement of goods and resources between countries and continents, thus supporting livelihoods while fostering development and connectivity. However, their strategic location at the land-sea interface makes them highly susceptible to climate-related changes (Izaguirre et al., 2020). This susceptibility leads to ports' increased vulnerability, which is further exacerbated by the design and condition of port infrastructure and facilities, dependence on external systems, such as telecommunications and socioeconomic factors including the role of each port in national economy and security (Chalastani et al., 2023). Rising sea levels, increased storm intensity and frequency, as well as changes in temperature and weather patterns are among the most pressing climate-related threats to ports. These changes result in hazards such as flooding, erosion and heatwaves that jeopardize the structural condition of the port itself, the undisrupted operation of the supply chain and the lives of adjacent coastal communities (Becker et al., 2016; Ng et al., 2018). Such hazards can cause damage to port infrastructure and equipment, disruption of port operation and logistics including greater downtime and port closures, higher insurance costs for port operations, permanent loss of land and severe threats to human health and well-being (Chhetri et al., 2014; Becker et al., 2013). Multiple climate-change induced events have caused severe damage to ports throughout the years, leading to economic losses, infrastructure destruction, and long-term disruptions to global supply chains. Among them, hurricane Katrina, one

of the most devastating hurricanes in U.S. history, struck the Gulf Coast in August 2005 and caused severe damage to the port of New Orleans. Flooding and storm surges inundated the port's infrastructure, resulting in extensive damage to terminals, warehouses, and equipment and massive economic losses in trade caused by operations' shut-down. In 2020, severe droughts and heatwaves significantly lowered water levels in the Panama Canal, a critical international shipping route. Restrictions were placed on the amount of cargo ships could carry, leading to delays and higher costs for shipping companies and to disruption of the global flow of goods between the Atlantic and Pacific Oceans.

In response to these challenges, the present research focuses on the main function of ports, i.e., the provision of shelter from waves, which ensures safe berthing, loading, and unloading of vessels, and examines how this function may be affected by climate change. While this topic has gained attention in recent years, published research on the subject remains limited. Casas-Prat and Sierra (2010) studied the long-term alterations in wave storminess patterns, based on hindcast data, along the Catalan coast (northwestern Mediterranean Sea) and provided as an example of the potential implications of climate change the changes of average wave agitation at Tarragona Port, emphasizing the importance of accounting for changes in wave direction. Sierra et al. (2015) analyzed the impact of climate change-induced changes in wave patterns, based on the A1B scenario of the 4th Assessment Report from the Intergovernmental Panel on Climate Change (IPCC, 2007) on harbor agitation at 13 ports along the Catalan coast. Their findings indicated a general slight reduction in the annual average agitation for most ports, although some areas experienced a minor increase. Sierra et al. (2017) examined how climate change affects wave agitation at the Port of Barcelona, using the RCP8.5 scenario from the IPCC's 5th Assessment Report (Church et al., 2013) and analyzing three distinct Sea Level Rise (SLR) projections. Their results indicated that changes in wave agitation solely due to wave patterns would be minimal, with a general trend toward a slight decrease. Conversely, the effects of SLR and the resulting increase in water depth are expected to enhance the penetration of waves into the harbor. Campos et al. (2019) proposed a downscaling methodology for addressing local effects at port scale and evaluating the operational vulnerability with an application at the Port of Gijón (Spain). Camus et al. (2019) proposed a hybrid statistical-dynamical framework for providing a probabilistic evaluation of port operability to assess a minimum level of downtime of the port and for introducing climate change in the assessment of wave agitation, at the Port of Candás (northwest Spain). They determined that the number of non-operational hours increases when comparing present conditions to future projections. Winckler et al. (2022) investigated the economic costs due to operational downtime and wave overtopping (under the RCP 8.5 scenario) at seven Chilean ports. Their results showed that some ports would reduce and others increase downtime for mid-century projections due

to local effects, but by the end-of-century, all ports would experience a reduction in downtime. Sierra et al. (2023) investigated the effects of climate change on the berthing areas of the Balearic Islands (Western Mediterranean Sea) ports, considering the RCP4.5 and RCP8.5 scenarios (AR5). They found that climate change will not generate significant changes in wave agitation due to negligible variations in wave patterns under future scenarios.

The studies mentioned above provide valuable insights into changes in wave agitation and operational downtime at port basins; however, research on this topic remains limited. Most available studies focus on the Spanish coasts, particularly within the western Mediterranean Sea, while, to the authors' knowledge, no similar investigations have been conducted for the eastern Mediterranean. For this specific region, Kollias et al. (2023) presented preliminary results from the current research, specifically assessing the impact of climate change on wave agitation at the Port of Piraeus, Greece. However, their analysis considered two different climate scenarios (RCP4.5 and RCP8.5) for future changes in offshore wave climate, but did not account for the effect of SLR.

Furthermore, despite the significant in recent studies addressing the risk (Izaguirre et al., 2021) and the vulnerability of ports (Li et al., 2025; McIntosh and Becker, 2020; 2019; Abdelhafez et al., 2021; Hsieh et al., 2013) few of them have considered the combined effects of SLR and shifts in incident wave climate, leading to an underestimation of vulnerability assessments (Sierra et al., 2023). The aim of the present study is to inform the work conducted for one of the nine project demonstrators of the European Commission's Horizon 2020 ARSINOE project (https://arsinoe-project.eu/), particularly the case study of "Mediterranean ports". The main task was to identify the state of the two ports' vulnerability. To do so, part of the work, hereto presented, is to investigate changes in the mean annual wave agitation patterns and berth downtime within two major port basins in the eastern Mediterranean, i.e., the passenger and cruise terminal of the Port of Piraeus in Greece and the Port of Limassol in Cyprus, under two different climate scenarios (RCP4.5 and RCP8.5) up to the year 2100. The analysis considers changes in offshore wave climate both with and without SLR to assess the specific role of rising sea levels in wave agitation changes.

The structure of the paper is as follows: Section 2 describes the study areas, methodology, data used, scientific background, and the setup of the numerical model implemented. Section 3 presents and discusses the offshore wave climate and wave agitation patterns in the two study areas over the coming decades. Finally, Section 4 summarizes the conclusions.

2 Study areas, methodology and numerical model

2.1 Study areas

Two major ports in the eastern Mediterranean Sea have been selected for the current investigation, the Port of Piraeus in Greece and the Port of Limassol in Cyprus.

2.1.1 The Port of Piraeus

The Piraeus Port is located (37°56'14"N; 23°37'16"E) in the region of Attica (approximately 10 km southwest of Athens) on the Saronic gulf (Fig. 1). It is the largest port in Greece and one of the largest ports in the Mediterranean, playing a crucial role in the development of international trade as well as the local and national economy, due to its strategic geographical position (situated close to the international trade routes, at the crossroads of Asia, Africa and Europe) and infrastructure (e.g., it possesses the necessary infrastructure for the accommodation of transshipment cargo and it is capable of serving even the largest modern container ships). Piraeus Port has a range of activities concerning the commercial and central ports, connects continental Greece with the Aegean islands, acts as an international cruise center and a commercial hub for the Mediterranean, providing services to more than 24,000 vessels, annually, of various types and sizes. Among others, the port serves various functions, including a container terminal, a car terminal, a passenger and cruise terminal, a ship repair zone, and dry dock facilities. The passenger and cruise terminal is specifically under scrutiny in the present research, as it is considered one of the largest in the world in respect to passenger traffic with a throughput volume of more than 20 million passengers per annum. The terminal is divided into areas that serve coasting and cruising (with over two million cruise passengers per year and capability of accommodating even the largest cruise ships).

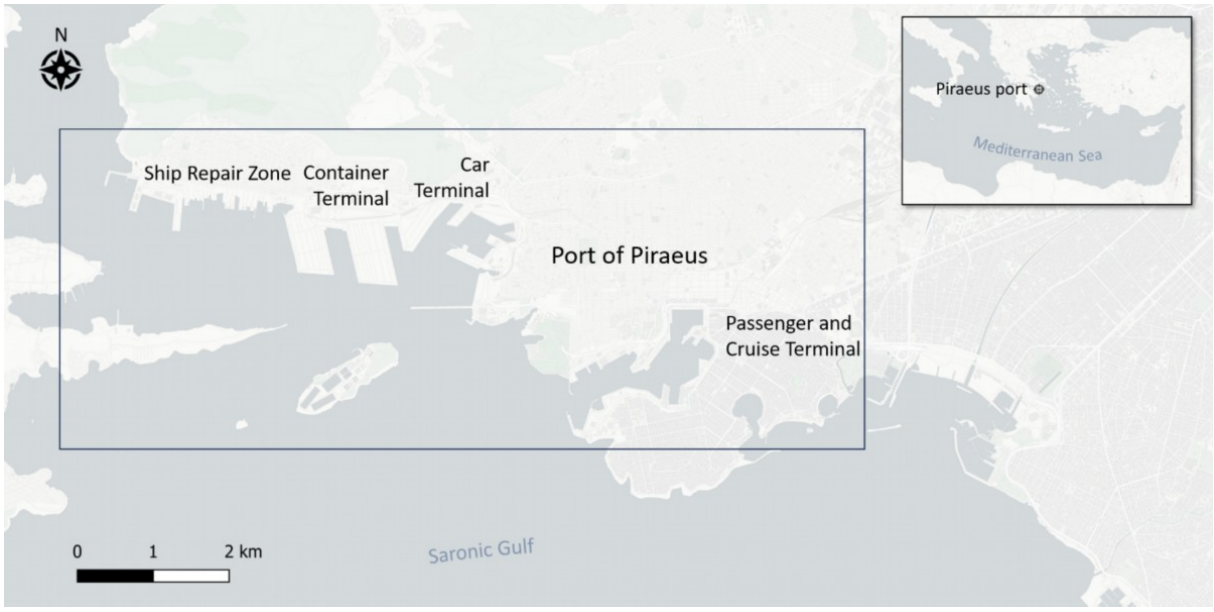

Fig. 1. Location of passenger and cruise terminal within Piraeus Port.

The quay wall of the passenger port extends over 9 km and features numerous berthing positions for passenger and cruise ships (11 positions for simultaneous berthing and a maximum draft of 11 m, Fig. 2). For the purposes of this study, five specific berthing positions, referred to as Evaluation Areas (EA) for the Port of Piraeus (EAPs), were selected for wave agitation analysis. These areas were selected based on the types of vessels they accommodate, their location within the basin, and the occupancy rates of each berth. The EAPs are illustrated in Fig. 2. EAP1 (295 m x 40 m) and EAP2 (280 m x 40 m) are designated for cruise ships, while EAP3 (175 m x 25 m), EAP4 (215 m x 25 m), and EAP5 (140 m x 25 m) serve passenger ships. The dimensions of each EA were determined based on the typical size of the ships accommodated in these areas. The port basin is protected by two breakwaters: the northern and southern breakwaters, which have lengths of approximately 240 meters and 460 meters, respectively (see Fig. 2). The outer sections of the breakwaters are constructed with a rubble mound, while the remaining sections feature a vertical front. Rocky formations are present along the adjacent coastlines.

The port is situated in a microtidal environment, with a mean tidal range close to 9 cm, as recorded by the tide gauge installed within the port and operated by the Hellenic Navy Hydrographic Service. Given the general geomorphology of the wider area and the incident wave climate, the port is primarily exposed to waves originating from the South-Southeast (150°N), South (180°N), South-Southwest (210°N), and West-Southwest (240°N).

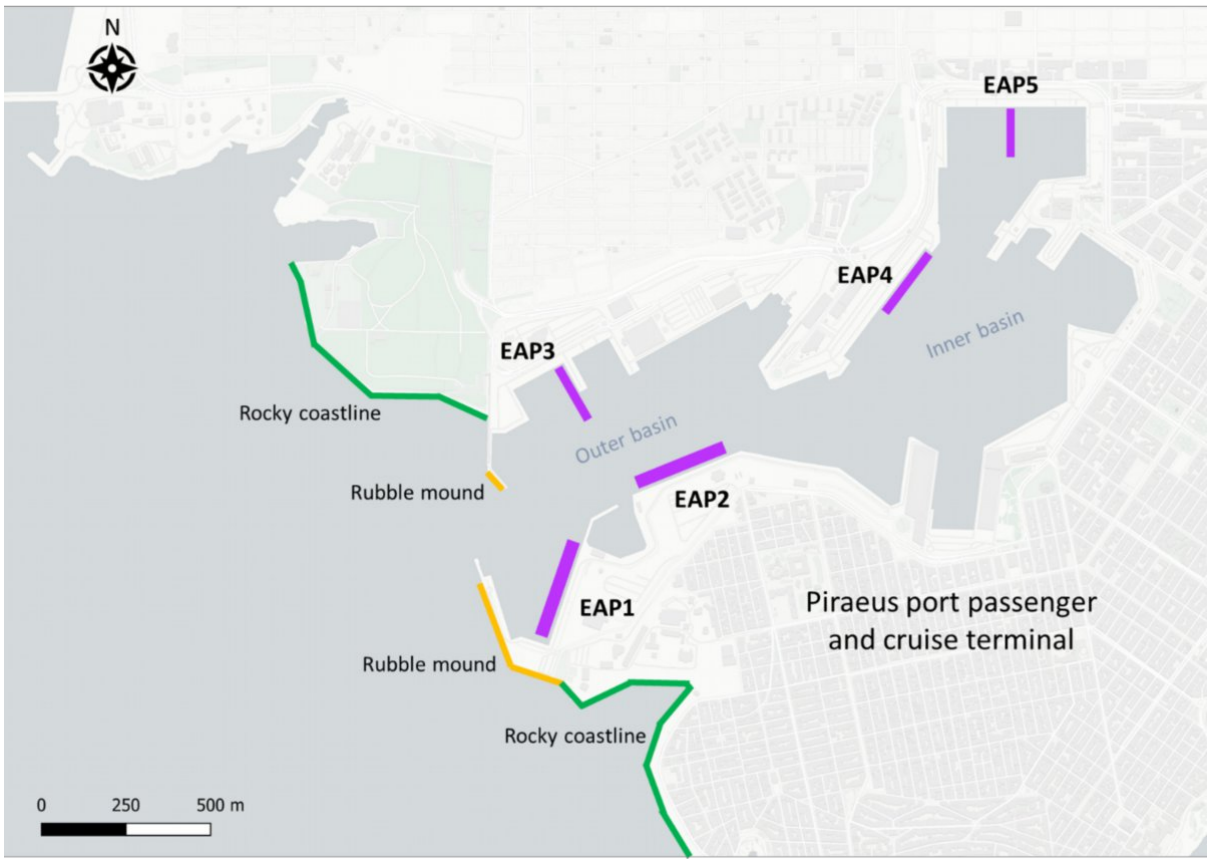

Fig. 2. Chosen Evaluation Areas (EAP1 to EAP5, highlighted in purple) for the Piraeus Port; outer sections of the breakwaters constructed with a rubble mound (in orange) and rocky formations along the adjacent coastlines (in green).

2.1.2 The Port of Limassol

The Limassol Port is located (34°38'58"N; 33°0'58"E) along the southern coast of Cyprus in the eastern Mediterranean (Fig. 3). The Port of Limassol is a multi-use port and is the main port of Cyprus and considered as one of the largest and busiest ports of the Mediterranean. The port serves various activities, including a cruise terminal, RoRo, general cargo and oil and gas logistics services. Its port sea area covers an area of one sq.km. and the land area covers an area of 1.3 sq.km. The quays have a total length of approximately 2 km, with a maximum draft of 16 m.

Fig. 3. Limassol Port in the eastern Mediterranean Sea.

Similarly to the Port of Piraeus, five Evaluation Areas in the Port of Limassol (EAL) were selected for wave agitation analysis as illustrated in Fig. 4. EAL1 and EAL2 (200 m x 30 m) accommodate containers, EAL3 cruise ships (350 m x 40 m) and EAL4 (120 m x 35 m) and EAL5 (160 m x 25 m) various types of vessels. The port basin is protected by two breakwaters: the windward (southern) breakwater, measuring approximately 2 km in length, and the leeside (northern) breakwater, which extends around 800 m. Sections of the breakwaters have been constructed with a rubble mound, while other parts have been reinforced with artificial concrete blocks.

This port is also located in a microtidal environment, with low mean tidal ranges of just a few centimeters, as observed over the past decades (although no formal measurements are available). Based on the general geomorphology of the surrounding area and the incident wave climate, the port is primarily exposed to waves coming from the East (90^0), East-SouthEast (120^0), South-SouthEast (150^0) and South (180^0).

Fig. 4. Chosen Evaluation Areas (EAL1 to EAL5, highlighted in purple) for the Limassol Port; outer sections of the breakwaters constructed with a rubble mound (in orange) and artificial concrete blocks (in light blue); adjacent natural beach (in yellow).

2.2 Methodology

The methodology employed in the current study is structured around four key steps, as outlined below and illustrated in Fig. 5.

Step 1. Data acquisition: In this step data regarding the offshore wave climate, the projected SLR and the bathymetry of the study areas were collected. Sea state datasets were obtained from the Copernicus Climate Change Service (C3S). In particular, ocean surface wave time series (Caires and Yan, 2020), for a period spanning from 1976 to 2100, derived from climate projections, are exploited. This dataset provides an understanding of the wave climate under the impact of climate change for the Northwest European Shelf and Mediterranean Sea. The ocean surface wave fields are computed using the ECMWF's Wave Model (SAW) forced by surface wind and accounting for ice coverage in polar latitudes. The wave climate is defined by means of the integrated wave spectral parameters such as the significant wave height and the peak wave period. In order to assess the impact of climate change on the ocean's surface wave field, the SAW model is run for three different climate scenarios: the current climate (also termed Reference, from 1976 to 2005), and two RCP scenarios, from 2041

to 2100, that correspond to an optimistic emission scenario where emissions start declining beyond 2040 (RCP4.5) and a pessimistic scenario where emissions continue to rise throughout the century often called the business-as-usual scenario (RCP8.5). The wave climate in these scenarios is simulated using wind forcing from a member of the EURO-CORDEX climate model ensemble - the HIRHAM5 regional climate model downscaled from the global climate model EC-EARTH. The horizontal coverage describes the European coastline along the 20 m bathymetric contour with a spatial resolution of 30 km and a temporal resolution of hourly records. The main variables that were used are the Significant Wave Height, H_s (m), the Peak Wave Period, T_p (s), and the Mean Wave Direction, MWD (clockwise from North in degrees). Moreover, data of SLR projections were obtained from the National Aeronautics and Space Administration (NASA) Sea Level Projection Tool (Fox-Kemper et al., 2021; Kopp et al., 2023; Garner et al., 2021) based on the IPCC's 6th Assessment Report (AR6). The chosen scenarios are the SSP2-4.5, that deviates mildly from a 'no-additional- climate-policy' reference scenario, resulting in a best-estimate warming around 2.7°C by the end of the 21st century relative to 1850-1900, and the SSP5-8.5, which is a high reference scenario with no additional climate policy. Finally, bathymetric data were obtained from recently conducted bathymetric surveys at the two ports, as provided by the port authorities.

Step 2. Pre-processing analysis: Before executing the wave agitation simulations, a pre-processing analysis is conducted to generate the necessary data and files. The available data, spanning the period from 2041 to 2100, is divided into two 30-year intervals: 2041–2070 and 2071–2100, for each RCP scenario. These datasets are then subjected to statistical analysis to determine the mean annual offshore wave climate for each port, RCP scenario, and 30-year period. This is done by categorizing the wave characteristics into 30-degree directional bins (12 sectors) and grouping wave heights in 0.5-meter increments. The mean significant wave height within each directional bin and wave height group, along with the corresponding mean peak period for the relevant wave directions, forms the basis for the scenarios to be simulated. These scenarios are modeled both with and without considering SLR, to assess the impact of rising sea levels on wave agitation. For this purpose, the average SLR projections, derived in the previous step, are applied for each 30-year interval (2041–2070 and 2071–2100). Additionally, the Evaluation Areas, i.e., specific berthing positions, are identified (Fig. 2 and 4) based on the types of vessels they accommodate, their location within the basin, and the occupancy rates of each berth. Lastly, a bathymetric grid is constructed for each port, along with a supplementary grid representing the anticipated wave reflection from each waterfront type (e.g., vertical seawalls, rubble mound or artificial block breakwaters, rocky coastlines, natural beaches, etc.), to be used as input for the numerical model (Chondros et al., 2024a).

Step 3. Simulations: With the wave and SLR scenarios defined, numerical simulations are carried out. The selected wave scenarios are used as input to the numerical wave model to simulate the propagation and transformation of waves from offshore to nearshore, as well as the resulting wave agitation within the port basin.

Step 4. Post-processing analysis: In the final step, a comparative analysis is conducted to highlight changes in the agitation patterns within the port basin over the coming decades. This analysis provides critical insights into the future operability of port infrastructure, helping to prepare for the new conditions driven by climate change. The mean annual downtime for each Evaluation Area is calculated based on the numerical modelling results, along with the frequency of occurrence of each simulated sea-state, in comparison to acceptable tolerance limits, as defined by widely accepted guidelines and recommendations (e.g., ROM 3.1-99, 2000; PIANC 2014). In this study, the maximum acceptable significant wave heights H_s (m) at berth are set at 0.50 m for container ships and 0.70 m for passenger ships and other type of vessels, ensuring safe operations under future wave conditions. The wave height in each EA is calculated as the average of the highest one-tenth of significant wave heights within that EA.

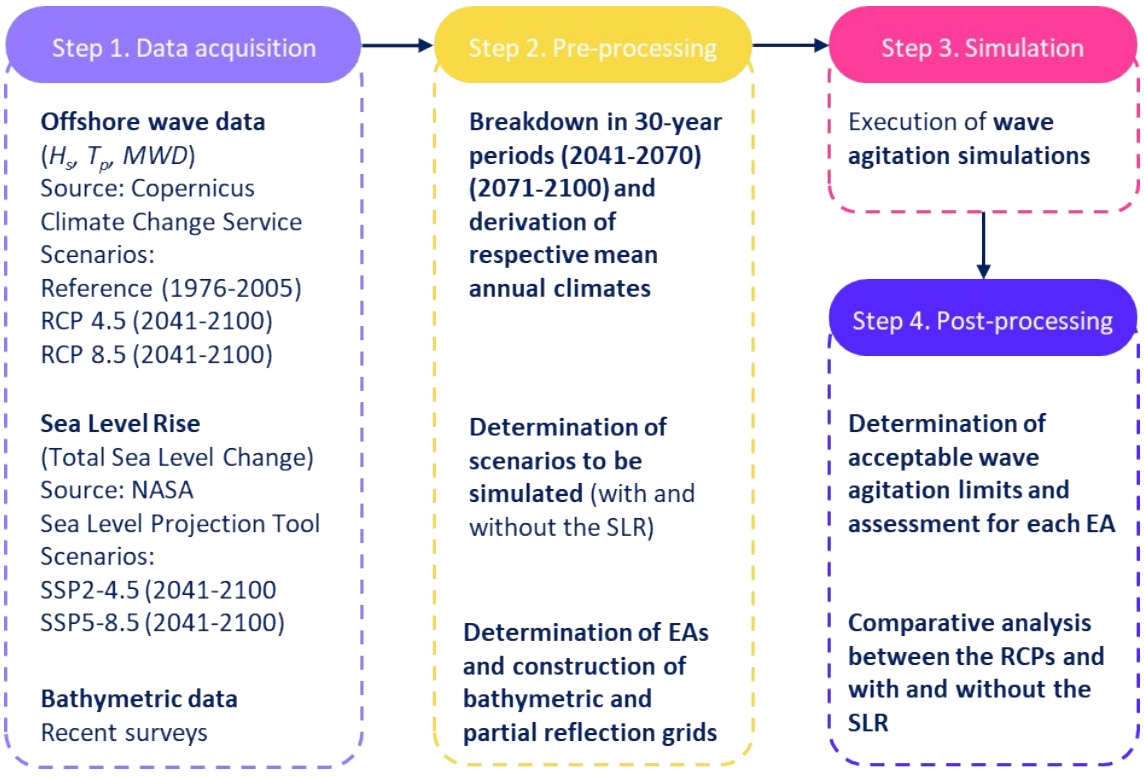

Fig. 5. Methodological key steps.

The methodology presented herein can be easily implemented for any port to assess changes in mean annual wave agitation and the downtime of berthing positions due to climate change. However,

certain limitations must be noted. Specifically, the drivers considered in this study for wave agitation are wave climate and SLR. Other factors, such as wind action, storm surges, and nearshore currents, which could affect the results, are not considered. Additionally, it is assumed that the water depths within and outside the port, as well as the port's layout, will remain unchanged. In the case of new construction works, the analysis would need to be revisited with those structures in place. Furthermore, the model used has not been calibrated with field measurements. Ideally, simultaneous wave measurements both inside and outside the port would significantly improve the reliability of the results, but such data is rarely available. Lastly, for ports located within enclosed bays, it is necessary to simulate wave propagation from deeper waters outside the bay to the vicinity of the port before conducting further analysis.

2.3 Numerical model's background and setup

The present study utilizes the nonlinear irregular wave propagation model Maris HMS (a Hyperbolic Mild-Slope model), developed by Scientia Maris (2022). It is an advanced nonlinear model which is based on the solution of mild-slope equations of hyperbolic approach and can simulate the spatiotemporal transformation of complex wave fields in harbours and coastal areas over uneven bottoms. It is capable of accurately simulating the simultaneous presence of all dominant phenomena occurring in a coastal field, such as: nonlinear irregular wave propagation, shoaling, refraction, diffraction, partial or total reflection and energy dissipation due to bottom friction and depth-induced wave breaking. This model is suitable for conducting wave disturbance studies in closed sea areas (gulfs, port basins) and simulating the presence of resonance and seiching phenomena in a port (Chondros et al., 2024a). Based on the works of (Chondros et al., 2021; 2024a, b), the continuity and momentum equations with energy dissipation terms are as follows:

$$\frac{\partial \zeta}{\partial t} + \nabla \cdot (\boldsymbol{U}h) = - w_b \frac{\partial \zeta}{\partial t} \tag{1}$$

$$\frac{\partial (\boldsymbol{U}h)}{\partial t} + \frac{c^2}{n} \nabla (n\zeta) = v_h \nabla^2 \cdot \boldsymbol{U} - w_f \boldsymbol{U} \tag{2}$$

where ζ is the sea-surface elevation; h is the water depth; $\boldsymbol{U} = (U, V)$ is the mean velocity vector with U and V being the mean horizontal velocities in the x and y directions, respectively; c is the phase celerity; $n = (1/2 + kh/\sinh kh)$; k is the wave number; v_h is the horizontal eddy viscosity coefficient responsible for replicating partial wave reflection; and w_f denotes energy dissipation due to bottom friction, while w_b denotes energy dissipation due to depth-induced breaking. The model simulates irregular waves by applying the principle of linear superposition (Chondros et al., 2024a).

The model requires as input the incident wave characteristics, (H_s, T_p, MWD), the bathymetric grid, and it outputs the significant wave height distribution throughout the entire domain. The wave

characteristics are specified along the internal wave generation lines, while sponge layers are placed around the perimeter of the numerical domain to absorb wave energy that propagates out of the domain, thereby preventing reflection from boundaries. Each simulation runs until a steady state is achieved, meaning the wave characteristics across the entire domain no longer change over time.

The bathymetric grid for each port is constructed to accurately represent the bathymetry of both the port and the surrounding study area, with equal spatial steps of dx = dy = 2.5 m in the two horizontal dimensions (x- and y- axes). The constructed grid covers an area of approximately 4.5 km x 4.0 km for the port of Piraeus and 5.0 km x 5.5 km for the port of Limassol (see Fig. 6, the coordinates are given in local coordinate system). A separate bathymetric grid was constructed for each SLR scenario under investigation to accurately capture shoreline retreat in sloping fronts, rather than applying a uniform value across the domain.

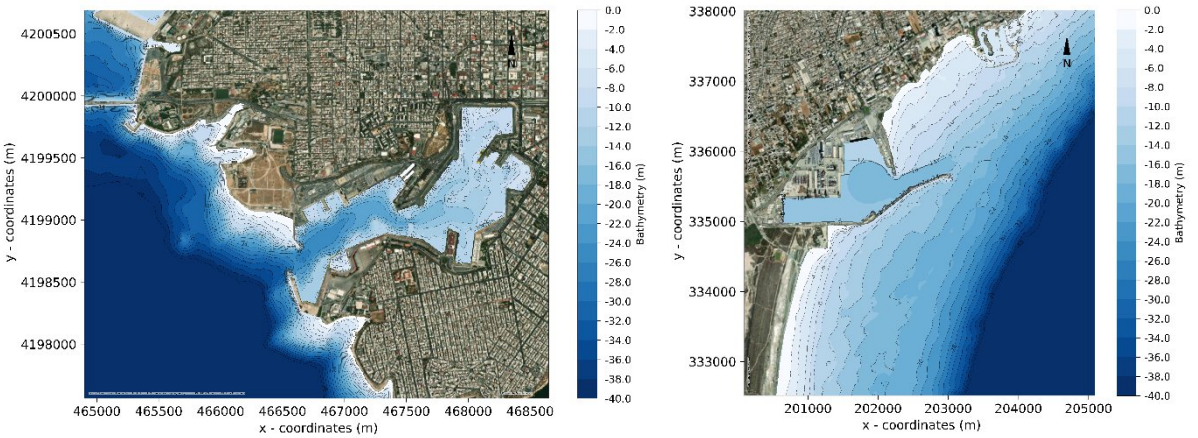

(a) Port of Piraeus (b) Port of Limassol

Fig. 6. Constructed bathymetric grids for ports under investigation.

To construct the eddy viscosity coefficient grid, for accurately simulating the partial reflection of waves across the diverse waterfront types (Fig. 2 and 4), the following steps were undertaken. First, the incident wave characteristics on the waterfront were estimated, and the anticipated wave reflection was determined using formulas derived from experimental datasets (such as Zanuttigh and van der Meer, 2008). The anticipated reflection coefficients are close to 1.0 for vertical quay walls, 0.55 for rubble mound breakwaters, 0.45 for artificial energy-dissipating concrete blocks, 0.3 for rocky shorelines and 0.15 for natural beaches. Next, for each sea-state scenario and waterfront type, the reflection coefficient was determined, and the corresponding value of the eddy viscosity coefficient, v_h, was obtained using an Artificial Neural Network (Chondros et al., 2024a). This Network takes as input the incident significant wave height, peak wave period, water depth at the waterfront, and the regularity or irregularity of the sea-state to produce the eddy viscosity coefficient values (for further

details, see Chondros et al., 2024a). Finally, the calculated eddy viscosity coefficients were compiled for each scenario into a separate file, which serves as input data for the mild-slope wave model. In this file, the eddy viscosity coefficient is set to zero throughout the numerical domain, except in the zones corresponding to the waterfronts' frontal areas, where partial wave reflection is expected.

3 Results and discussion

3.1 Offshore wave climate and water level data

Offshore wave climate data were sourced from the Copernicus Climate Change Service, specifically from the data package titled "Ocean Surface Wave Time Series for the European Coast from 1976 to 2100 Derived from Climate Projections." From this package, wave characteristic data were extracted,on an hourly basis, for locations offshore of the ports, specifically at WGS84 coordinates [37°53'59.9"N, 23°36'00.8"E] for the Port of Piraeus and [34°38'10.84"N, 33° 3'51.52"E] for the Port of Limassol. To quantify the frequency and height of waves by direction, tables and wave rose diagrams have been created for each port. MWD is provided as the direction that the wave is coming from, clockwise from North in degrees. MWD are broken down into 30-degree bins, i.e., 12 sectors in total (N, NNE, ENE, E, ESE, SSE, S, SSW, WSW, W, WNW, NNW) and significant wave heights are distributed into equally spaced groups of 0.5 m, i.e., [0, 0.5], (0.5-1.0], (1.0-1.5], etc.

The mean annual frequencies of occurrence, f (%), per wave height group and direction bin, along with the corresponding average wave heights and periods, are presented in Table 1 for the Reference period for the Port of Piraeus, as an example. It is noted that only the relevant directions are shown, specifically those to which the ports are exposed.

Table 1

Mean annual frequencies of occurrence and average heights and periods, per wave height group and per direction bin, for the Reference period (1976-2005) for the Port of Piraeus.

Wave Height Groups (m)	Mean Wave Direction											
	SSE (150°)			S (180°)			SSW (210°)			WSW (240°)		
	f (%)	H_s (m)	T_p (s)	f (%)	H_s (m)	T_p (s)	f (%)	H_s (m)	T_p (s)	f (%)	H_s (m)	T_p (s)
[0-0.5]	16.473	0.16	3.21	16.473	0.17	3.46	5.627	0.16	3.15	3.558	0.16	2.74
(0.5-1]	0.739	0.70	5.20	3.807	0.71	5.56	1.088	0.70	5.44	0.436	0.69	4.36
(1-1.5]	0.201	1.18	6.45	1.307	1.20	6.33	0.177	1.17	6.30	0.060	1.18	4.94
(1.5-2]	0.041	1.69	7.03	0.391	1.69	7.08	0.029	1.67	6.32	0.006	1.63	5.43
(2-2.5]	0.011	2.21	7.65	0.097	2.19	7.57	0.004	2.21	8.17	0.0004	2.13	5.80
(2.5-3]	0.003	2.70	8.74	0.024	2.72	8.05	0.001	2.77	8.22	–	–	–
(3-3.5]	0.001	3.24	9.87	0.008	3.21	8.84	–	–	–	–	–	–
(3.5-4]	0.001	3.68	10.16	0.003	3.73	9.15	–	–	–	–	–	–
(4-4.5]	–	–	–	0.001	4.19	10.08	–	–	–	–	–	–
(4.5-5]	–	–	–	0.001	4.78	10.23	–	–	–	–	–	–

(5-5.5]	–	–	–	0.004	5.18	9.93	–	–	–	–	–	–
	17.470			22.117			6.926			4.060		

Based on the tables for the Reference period, it is observed that for the Port of Piraeus, the prevailing wave direction is from S with an average annual frequency of occurrence of 22.117%, followed by the SSE with an average annual frequency of 17.470%. The SSW direction follows with 6.926%, and the WSW with 4.060%. The S direction also exhibits the largest waves, reaching the wave height group of (5-5.5] m, though with a very low frequency of occurrence (0.004%). For the other directions, wave heights offshore of the port remain below 4 m.

Similarly, for the Port of Limassol, the prevailing wave direction is the WSW with an average annual frequency of 37.003%, followed by the W at 30.631%. However, these directions do not significantly impact the wave agitation within the port. The directions that do influence the port are the E, with the highest mean annual frequency among them, at 7.585%, followed by the ESE at 2.170%, the SSE at 1.951%, and the S at 1.769%. Among these four directions of interest, the E also exhibits the largest waves, reaching the (4-4.5] m group, though with an extremely low frequency of occurrence (0.0004%). For the remaining directions, wave heights offshore of the port remain below 3.5 m.

To quantify the changes in the offshore wave climate, similar tables have been prepared for each RCP scenario and 30-year period, for both ports, as well as wave rose diagrams, representing the mean annual wave climate for the two ports, as illustrated in Fig. 7.

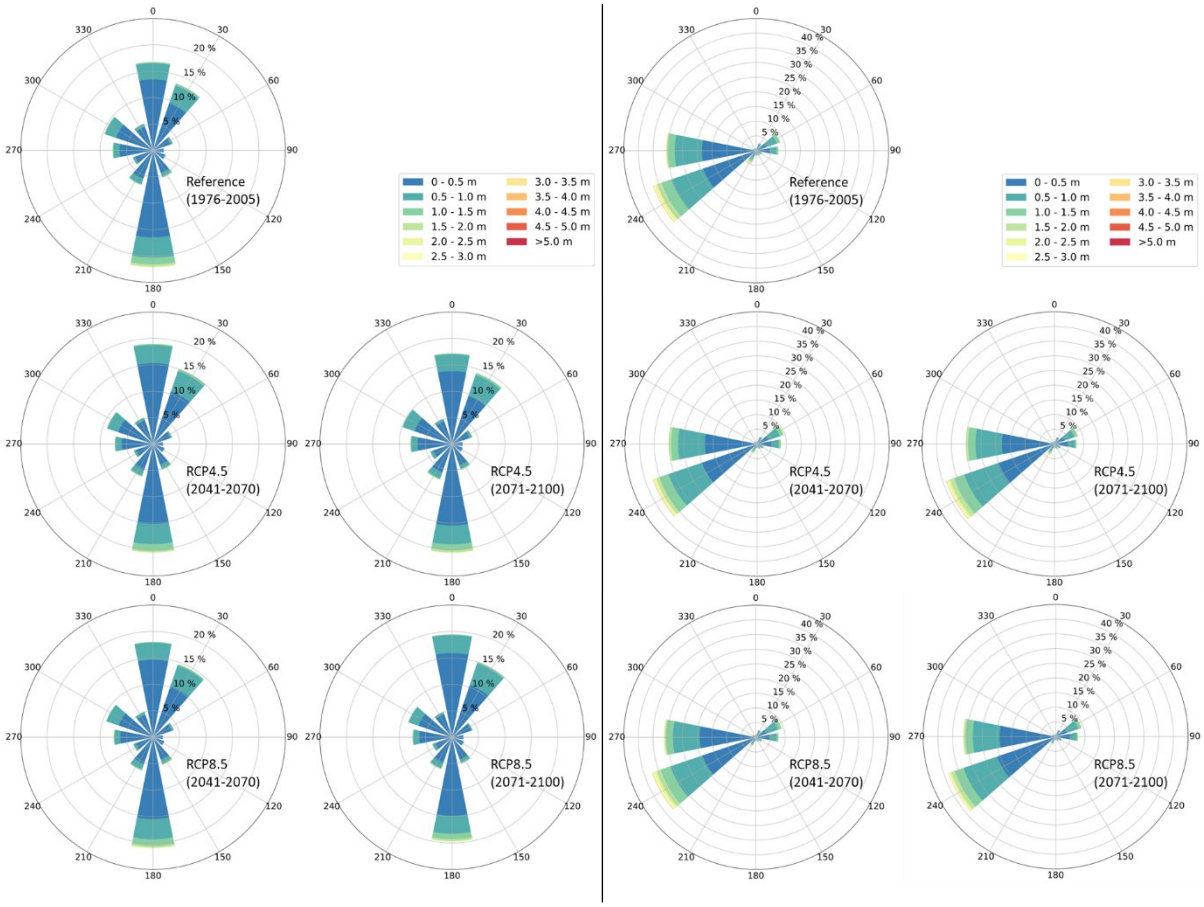

(a) Port of Piraeus (b) Port of Limassol

Fig. 7. Reference and projected offshore wave rose diagrams.

An inspection of the wave rose diagrams, reveals no significant changes for either the Port of Piraeus or the Port of Limassol across any of the RCP scenarios or the two 30-year periods examined. To enable a more in-depth investigation, the following figures were produced. Figure 8 illustrates the mean annual wave characteristics, including wave height, peak period, and mean direction for each direction of interest for both ports. Regarding wave height, for the Port of Piraeus, a notable increase is observed in the first of the four directions of interest, i.e. the SSE, rising from 0.2 m to approximately 0.3 m across all RCP scenarios, which could potentially impact wave agitation within the port basin. However, it should be noted that due to the layout of the windward and leeside breakwaters, forming the orientation of the port entrance, this direction generates the least disturbance in the basin. For the remaining directions, the predicted mean wave heights remain close to the values of the Reference period, with minor fluctuations. For the Port of Limassol, a slight reduction in mean wave height is observed across all RCP scenarios for all directions except the East. As for the peak period and mean direction, the projections remain closely aligned with the Reference period for all RCP scenarios and both ports.

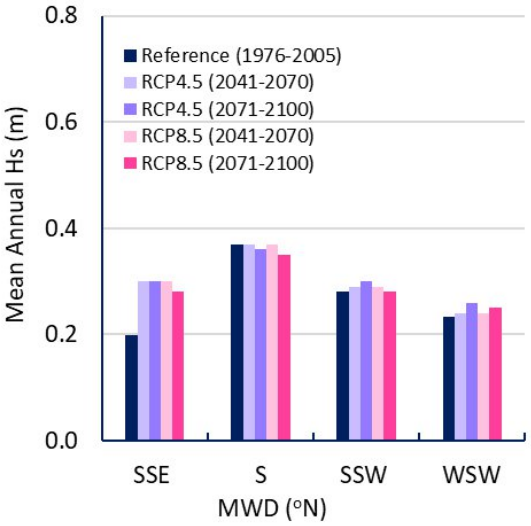

(a) Mean annual wave height, Port of Piraeus

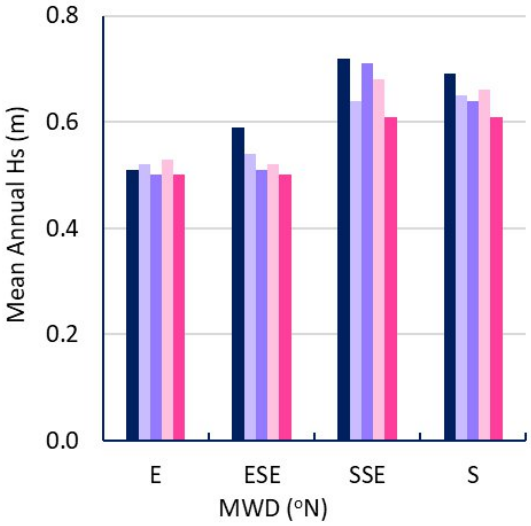

(b) Mean annual wave height, Port of Limassol

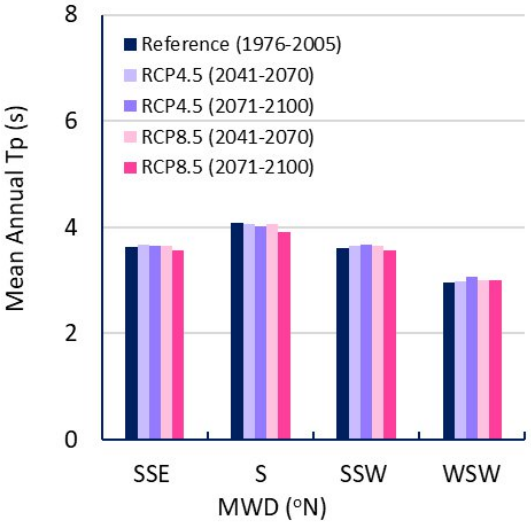

(c) Mean annual peak period, Port of Piraeus

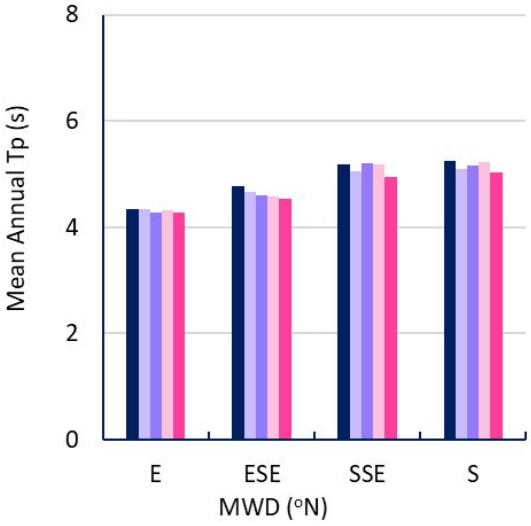

(d) Mean annual peak period, Port of Limassol

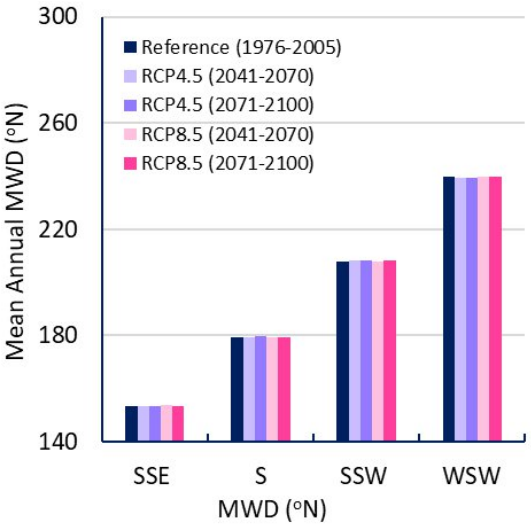

(e) Mean annual MWD per direction bin, Port of Piraeus

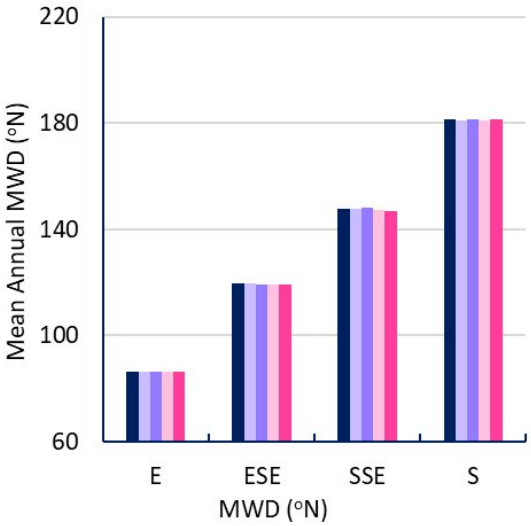

(f) Mean annual MWD per direction bin, Port of Limassol

Fig. 8. Mean annual wave characteristics per direction for the Reference period, RCP4.5 and RCP8.5.

Fig. 9 depicts the mean annual frequency of wave height occurrence per direction of interest for the Reference period, and for both RCP scenarios and future time periods, for both ports. It is observed that in most directions, the mean annual frequency of projected values compared to Reference ones remains relatively stable or shows a slight decrease, averaging 0.5% lower than the Reference period, with a maximum reduction of 2.4% in the S direction for RCP8.5 during the 2071–2100 period. The only increases are observed under the RCP4.5 scenario for the 2071–2100 period in the SSW and WSW directions, with values 0.2% and 0.3% higher than the Reference data, respectively. For the Port of Limassol, the projected mean annual frequencies also remain relatively consistent with minor decreases or increases. However, for the E and ESE directions, all RCP scenarios for both periods show increases of approximately 0.2% compared to the Reference period, while for the SSE and S directions, a decrease of around 0.3% is observed.

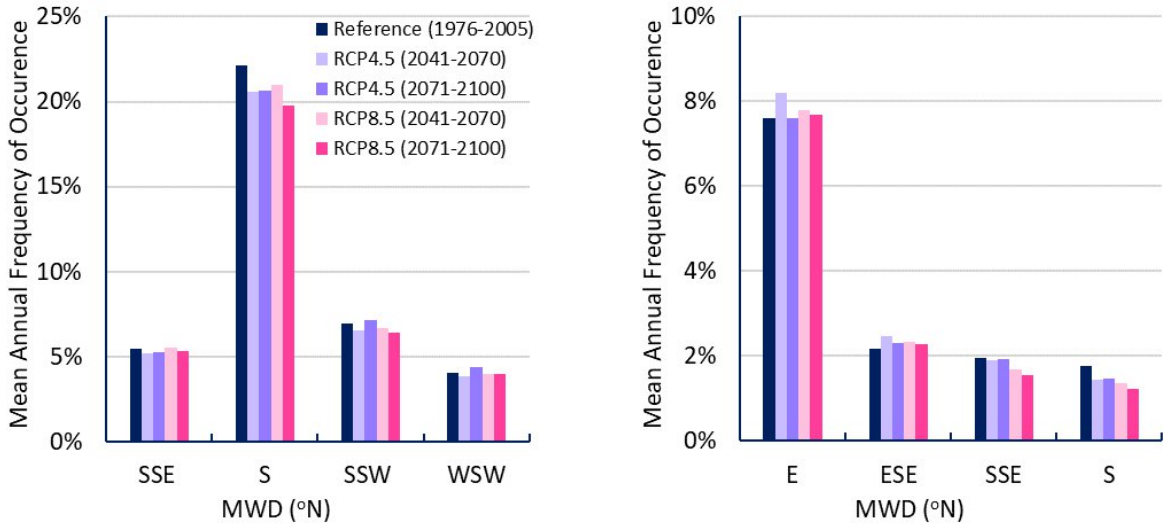

(a) Port of Piraeus (b) Port of Limassol

Fig. 9. Mean annual frequency of wave height occurrence per direction for the Reference period, RCP4.5 and RCP8.5.

Furthermore, Figs. 10 and 11 present the mean annual frequency of wave height occurrence per wave height group for all directions of interest. For the Port of Piraeus (Fig. 10), it is observed that the mean annual frequency decreases across all directions of interest for the wave height group [0–0.5] m, with a lower frequency of 1.8%, on average, compared to the Reference period (Fig. 10a). The groups up to 2 m, remain relatively similar, while some changes are observed in groups with wave heights greater than 2 m. Specifically, the (2–2.5] m and (2.5–3] m groups show a noticeable decrease for the RCP4.5 scenario during the 2041–2070 period compared to the Reference period, and an increase for the same RCP during the 2071–2100 period. It is also noteworthy that while the data of

the Reference period shows a few events across all wave height groups up to 5.5 m, the RCP projections limit occurrences to groups up to 3.5 m, except for RCP8.5 (2041–2070), which reaches the (4.0–4.5] m group. For the Port of Limassol, no significant changes are observed (Fig. 11). The only noteworthy variations include a slight decrease in the frequency of wave heights between 1 m and 2.5 m, and a minor increase in wave heights between 2.5 m and 3.5 m, consistently across all RCP scenarios and periods examined.

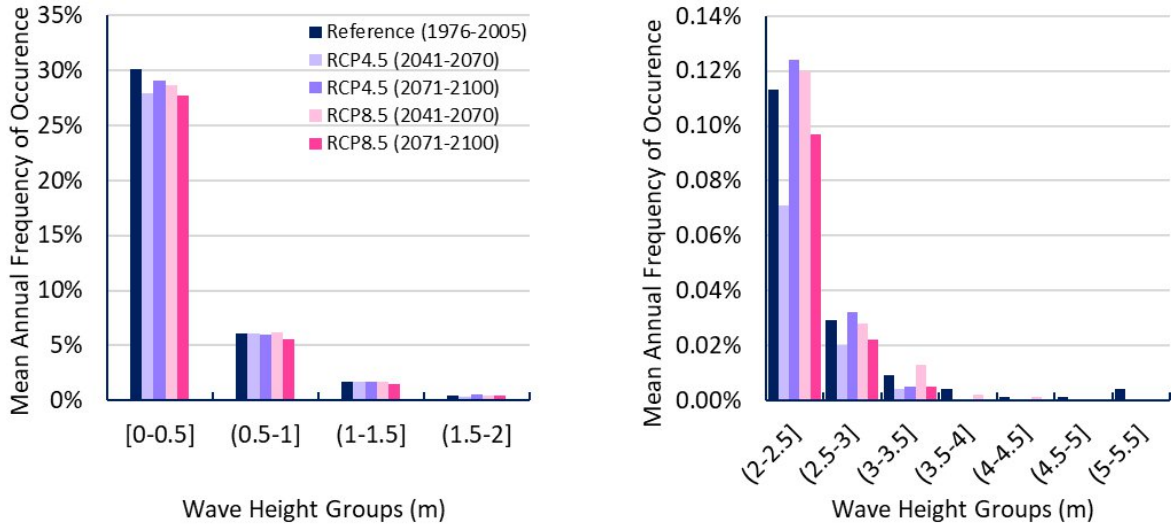

(a) Wave height groups [0, 2] m (b) Wave height groups (2, 5.5] m

Fig. 10. Mean annual frequency of wave height occurrence per wave height group from all directions of interest for the Reference, RCP4.5 and RCP8.5, for the Port of Piraeus.

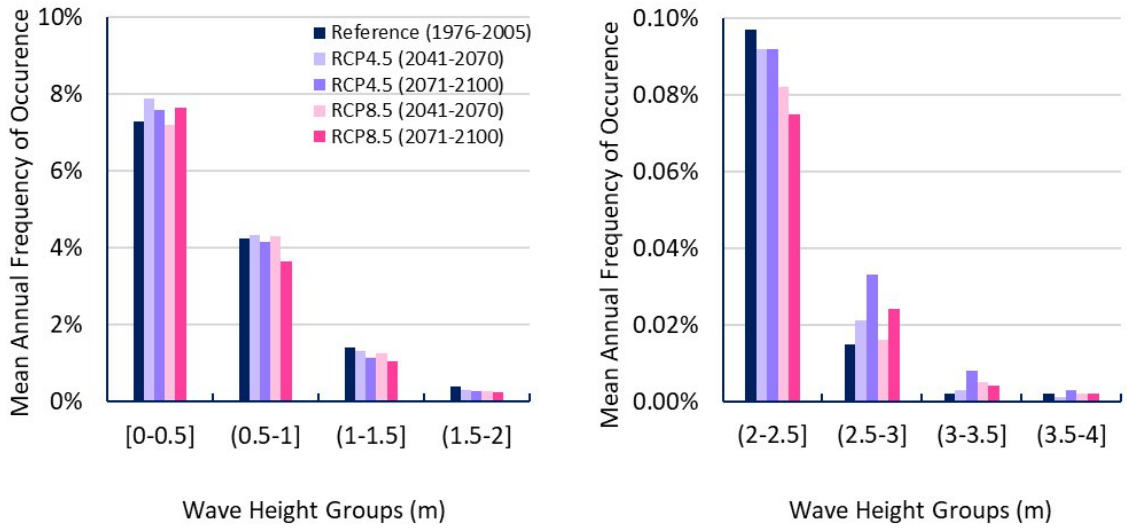

(a) Wave height groups [0, 2] m (b) Wave height groups (2, 4] m

Fig. 11. Mean annual frequency of wave height occurrence per wave height group from all directions of interest for the Reference, RCP4.5 and RCP8.5, for the Port of Limassol.

In addition to wave climate, SLR projections were obtained from NASA's Sea Level Projection Tool for each considered SSP scenario, covering the period from 2041 to 2100. The average SLR for each 30-year period, as given in Table 2, is considered in the current study. Notably, the projections appear more adverse for the Port of Limassol.

Table 2

Projected Sea Level Rise for each SSP scenario and 30-year period, for both ports.

Scenario	Period	SLR (Port of Piraeus)	SLR (Port of Limassol)
SSP2-4.5	2041-2070	0.15 m	0.27m
SSP2-4.5	2071-2100	0.30 m	0.48m
SSP5-8.5	2041-2070	0.19 m	0.31m
SSP5-8.5	2071-2100	0.42 m	0.62m

3.2 Wave agitation

Each wave event, as shown in Table 1 (indicatively for the Reference period of Piraeus), combined with the consideration of SLR for each RCP scenario and 30-year period (as presented in Table 2), constitutes a sea-state scenario (offshore wave characteristics and SLR) to be simulated. It is noted that no SLR was considered for the Reference period. In total, 224 simulation runs were conducted for the Port of Piraeus and 246 for the port of Limassol. Once the sea-state scenarios were defined, the corresponding bathymetric and eddy viscosity/partial reflection grids were constructed as previously described. The results for each port are discussed in the following sections.

3.2.1 Port of Piraeus

Figure 12 presents the simulation results for wave agitation in the Port of Piraeus, focusing on the largest waves that occurred during each period and under each RCP scenario, from the predominant direction, with the highest frequency of occurrence, namely the South. It is observed that the largest wave (H_s = 5.18 m, T_p = 9.93 s) from the dataset of the Reference period (1976-2005) generates the most significant disturbance within the port, affecting both the entrance and the outer harbor basin, with wave heights exceeding 2 m, as well as the inner basin. For the remaining scenarios, the disturbance is mainly confined to the entrance and the outer basin. Overall, it is noted that the passenger and cruise terminal of the Port of Piraeus is relatively well protected, with the outer basin being more susceptible to wave agitation, while the inner basin experiences lower agitation levels. Nevertheless, extreme wave events originating from the south can significantly impact the entire port basin, generating high wave heights, albeit with a very low annual frequency.

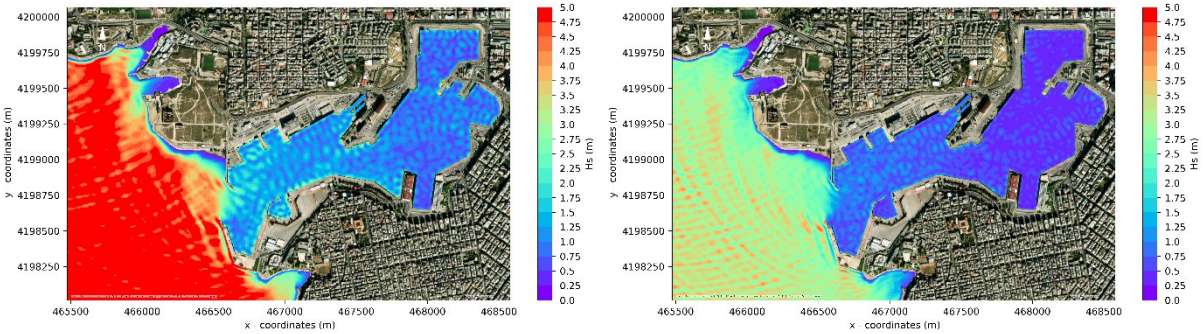

(a) Incident wave characteristics: H_s = 5.18 m, T_p = 9.93 s, MWD = 184°; SLR = 0.00 m (Reference, 1976-2005).

(b) Incident wave characteristics: H_s = 3.16 m, T_p = 8.34 s, MWD = 189°, SLR = 0.15 m (RCP4.5, 2041-2070).

(c) Incident wave characteristics: H_s = 4.08 m, T_p = 9.16 s, MWD = 169°; SLR = 0.19 m (RCP8.5, 2041-2070).

(d) Incident wave characteristics: H_s = 3.16 m, T_p = 8.63 s, MWD = 182°; SLR = 0.42 m (RCP8.5, 2071-2100).

Fig. 12. Spatial distribution of wave heights for various individual incident wave scenarios, for the Port of Piraeus.

After completing the simulations for each incoming sea-state scenario, covering all wave height groups and directional bins, both for the reference period and the RCP scenarios, a post-processing analysis was conducted to calculate the mean annual agitation in the port basin. Specifically, the numerical grid for each considered incident sea-state scenario was multiplied by the corresponding mean annual frequency of occurrence (as shown in Table 1), and then these weighted grids were summed to derive the mean annual agitation for each period and RCP scenario. The results are presented in Figure 13 for the reference period (1976-2005), RCP4.5 (2041-2070, SLR = 0.15 m), RCP8.5 (2041-2070, SLR = 0.19 m), and RCP8.5 (2071-2100, SLR = 0.42 m). It is observed that offshore of the port, the mean annual agitation is relatively higher than in any of the considered RCP scenarios. Within the port basin, a similar pattern is observed between the Reference period and the RCPs. However, a slight increase in the extent and intensity of agitation is noted for the RCPs, particularly at the port entrance, in the outer basin, and also in the inner basin. The same applies to RCP4.5 (2071-2100), which is not shown here.

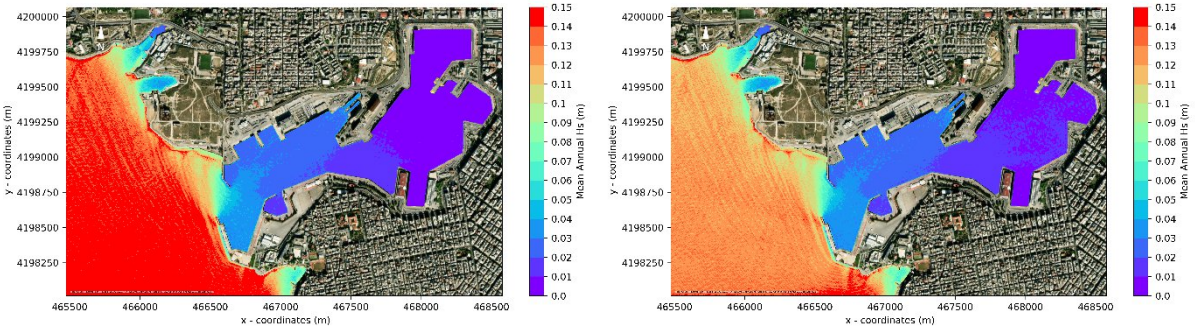

(a) Mean annual H_s for Reference period (1976-2005).

(b) Mean annual H_s for RCP4.5 (2041-2070, SLR = 0.15 m).

(c) Mean annual H_s for RCP8.5 (2041-2070, SLR = 0.19 m).

(d) Mean annual H_s for RCP8.5 (2071-2100, SLR = 0.42 m).

Fig. 13. Mean annual H_s for various scenarios, for the Port of Piraeus.

To draw more solid conclusions, additional grids and figures were generated. Specifically, Fig. 14 presents the difference in mean annual agitation between the RCP scenarios and the reference period. For instance, the difference (in meters) is given by $Difference = \left(\text{Mean annual } H_s^{\text{RCP4.5 (2041–2070)}} - \text{Mean annual } H_s^{\text{Reference (1976–2005)}}\right)$. It is observed that in the area outside the port, this difference is negative for all RCPs, indicating that the average wave height during the reference period in this region is higher. Within the port, which is of primary interest, there is no clear trend of either a uniform increase or decrease across all RCPs and periods examined. For example, for RCP4.5 (2071-2100, SLR = 0.30 m, Fig. 14b), the difference is positive throughout most of the outer basin, suggesting an increase in mean wave agitation for this scenario. Conversely, in RCP4.5 (2041-2070, SLR = 0.15 m, Fig. 14a), a slight decrease is observed across nearly the entire outer basin, while for RCP8.5 (2041-2070 and 2071-2100, Figs. 14c and 14d, respectively), there are subareas showing both increases and decreases. Notably, in the inner basin, the differences are minimal, indicating that this area will likely remain unaffected. In light of these results, it can be concluded that climate change will not necessarily result in a consistent increase in wave agitation across all RCP scenarios; rather, it will depend on the specific RCP, the 30-year period, and the location within the port basin.

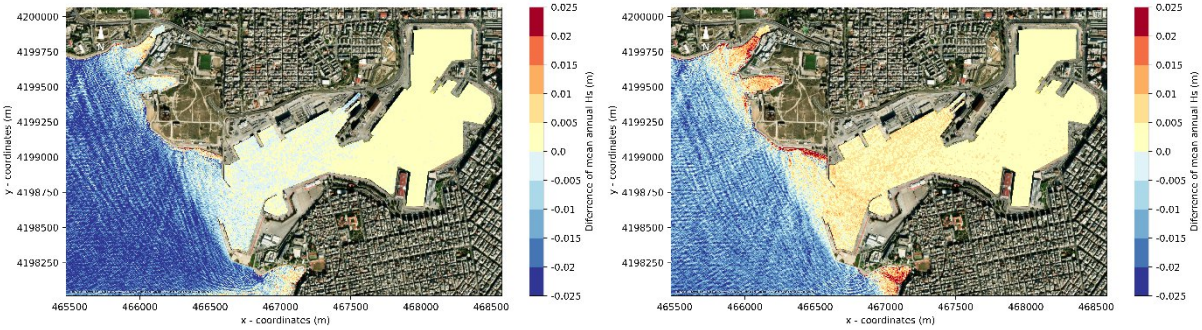

(a) Difference of mean annual H_s, between RCP4.5 (2041-2070, SLR = 0.15 m) and Reference period (1976-2005).

(b) Difference of mean annual H_s, between RCP4.5 (2071-2100, SLR = 0.30 m) and Reference period (1976-2005).

(c) Difference of mean annual H_s, between RCP8.5 (2041-2070, SLR = 0.19 m) and Reference period (1976-2005).

(d) Difference of mean annual H_s, between RCP8.5 (2071-2100, SLR = 0.42 m) and Reference period (1976-2005).

Fig. 14. Difference of mean annual H_s, between RCP scenarios and Reference period, for the Port of Piraeus.

To investigate the role of SLR in the changes to mean annual wave agitation, the differences between the RCP scenarios and the reference period were analyzed without considering SLR, focusing exclusively on changes in wave climate. As shown in Figure 15, both in the outer and inner basins, no significant changes are observed. However, the general trend shows a slight reduction in wave agitation across all RCPs, suggesting that SLR enhances wave agitation. To explore this further, an additional grid was created for each RCP scenario, representing the difference in mean annual agitation with and without SLR. As shown in Figure 16, these differences remain equal to or greater than zero, indicating that SLR contributes to slightly increased agitation, primarily in the outer basin.

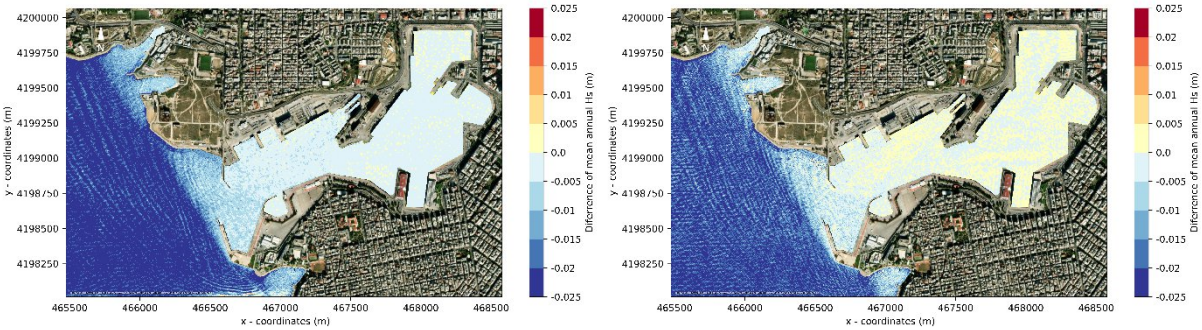

(a) Difference of mean annual H_s, between RCP4.5 (2041-2070, without SLR) and Reference period (1976-2005).

(b) Difference of mean annual H_s, between RCP4.5 (2071-2100, without SLR) and Reference period (1976-2005).

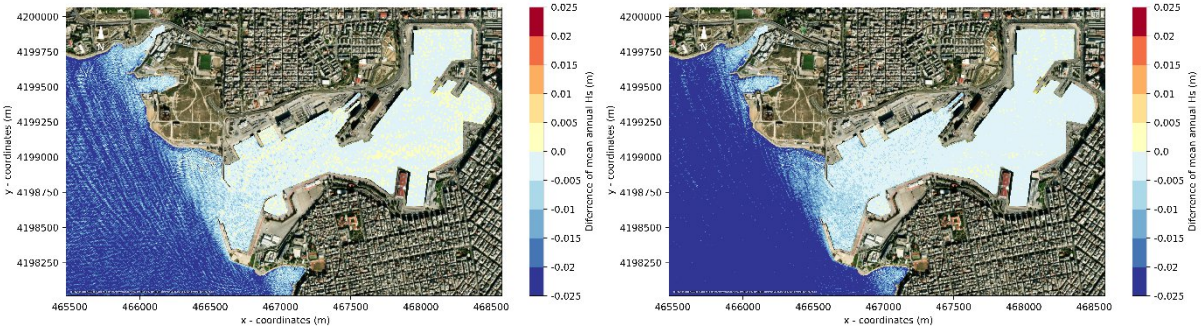

(c) Difference of mean annual H_s, between RCP8.5 (2041-2070, without SLR) and Reference period (1976-2005).

(d) Difference of mean annual H_s, between RCP8.5 (2071-2100, without SLR) and Reference period (1976-2005).

Fig. 15. Difference of mean annual H_s, between RCP scenarios, without considering SLR, and Reference period, for the Port of Piraeus.

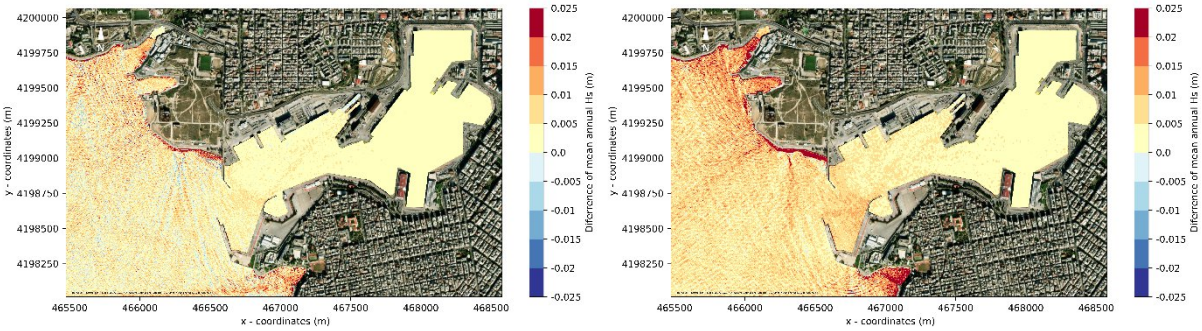

(a) Difference of mean annual H_s, for RCP4.5 (2041-2070), with and without considering SLR of 0.15 m.

(b) Difference of mean annual H_s, for RCP4.5 (2071-2100), with and without considering SLR of 0.30 m.

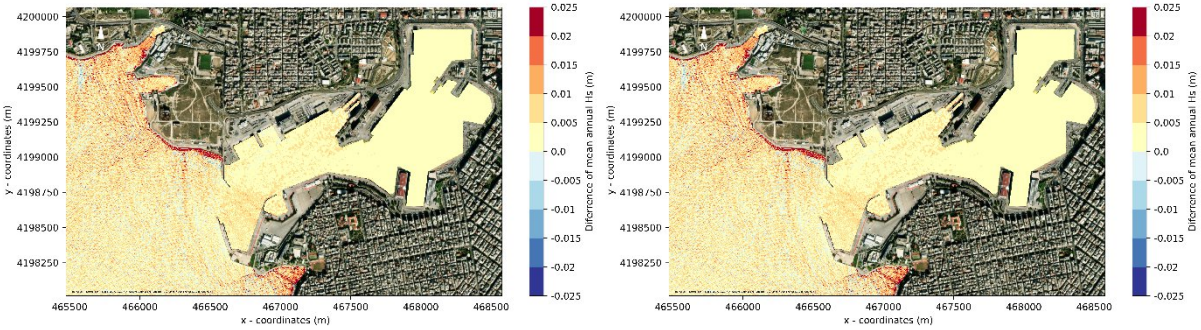

(c) Difference of mean annual H_s, for RCP8.5 (2041-2070), with and without considering SLR of 0.19 m.

(d) Difference of mean annual H_s, for RCP8.5 (2071-2100), with and without considering SLR of 0.42 m.

Fig. 16. Difference of mean annual H_s, for the investigated RCP scenarios, with and without considering the SLR, for the Port of Piraeus.

Along with the analysis of mean annual wave agitation across the entire basin, the mean annual downtime for each EA (berthing position, as defined in Fig. 2) was also examined. The following process was used to calculate downtime: For each simulated wave event, the agitation at each EA was first calculated as the average of the top 10% highest waves recorded at that area. If this value exceeded the allowable thresholds set in the methodology (e.g., 0.7 m for passenger and cruise ships), the corresponding mean annual frequency of occurrence for that event was considered as downtime. This process was repeated for all wave events, and the total frequencies were summed. The result was then multiplied by 365 days and 24 hours to estimate the mean annual downtime for all EAs, for

all RCP scenarios and the hindcast period, both with and without considering SLR. Table 3 and Figure 17 present the results. It is observed that the downtime for EAP1, EAP2, and EAP3, located in the outer basin, is expected to increase significantly, particularly under the RCP 4.5 (2071-2100) scenario, which appears to have the greatest impact. An increase is also anticipated for RCP 8.5 in both 30-year periods (2041-2070). A relatively small decrease is predicted for positions EAP1 and EAP2 under the RCP 4.5 (2041-2070) scenario only. For EAP4 and EAP5, located in the inner basin, a reduction in wave agitation is projected for all RCP scenarios considering SLR.

Regarding the contribution of SLR, no consistent trend is observed, as it can either increase, decrease, or have no impact on agitation. For example, at EAP1, the scenarios that do not account for SLR yield the same results as those that do, across all examined RCPs and periods. In contrast, under the RCP 8.5 scenario (2071-2100), there is a significant increase in downtime at EAP3 from 32.5 hours to 40.6 hours when SLR is considered. Conversely, for RCP 8.5 in both periods (2041-2070 and 2071-2100), a substantial decrease in downtime is observed at EAP2, from 22.2 hrs to 14.4 hrs and from 21.8 hrs to 13.6 hrs, respectively. This decrease is also noted at EAP3 under the RCP 4.5 (2041-2070) scenario, from 31.9 hrs to 27.1 hrs. This behavior does not align with the findings from the previous analysis of mean annual agitation across the entire basin, where it was observed that SLR does not lead to lower agitation levels. This discrepancy may be attributed to the fact that in this downtime analysis, specific high-energy wave events significantly impact downtime calculations when they exceed the allowable threshold, but due to their very low mean annual frequency, they do not substantially influence overall mean conditions.

Table 3

Mean annual downtime (in hours) per Evaluation Area and RCP scenario with and without (w/o) considering the SLR, for the Port of Piraeus.

Evaluation Areas	Reference (1976-2005)	RCP4.5 (2041-2070) SLR 0.15m	RCP4.5 (2041-2070) w/o SLR	RCP4.5 (2071-2100) SLR 0.30m	RCP4.5 (2071-2100) w/o SLR	RCP8.5 (2041-2070) SLR 0.19m	RCP8.5 (2041-2070) w/o SLR	RCP8.5 (2071-2100) SLR 0.42m	RCP8.5 (2071-2100) w/o SLR
EAP 1	9.9	9.6	9.6	24.7	24.7	22	22	13.6	13.6
EAP 2	12.4	9.6	9.6	24.7	24.7	22.2	14.4	21.8	13.6
EAP 3	21	31.9	27.1	45.8	45.9	40.5	40.5	32.5	40.6
EAP 4	2.2	0.8	2.2	0.8	0.8	1.1	2.7	0.2	<0.1
EAP 5	0.5	<0.1	<0.1	<0.1	<0.1	<0.1	<0.1	<0.1	<0.1

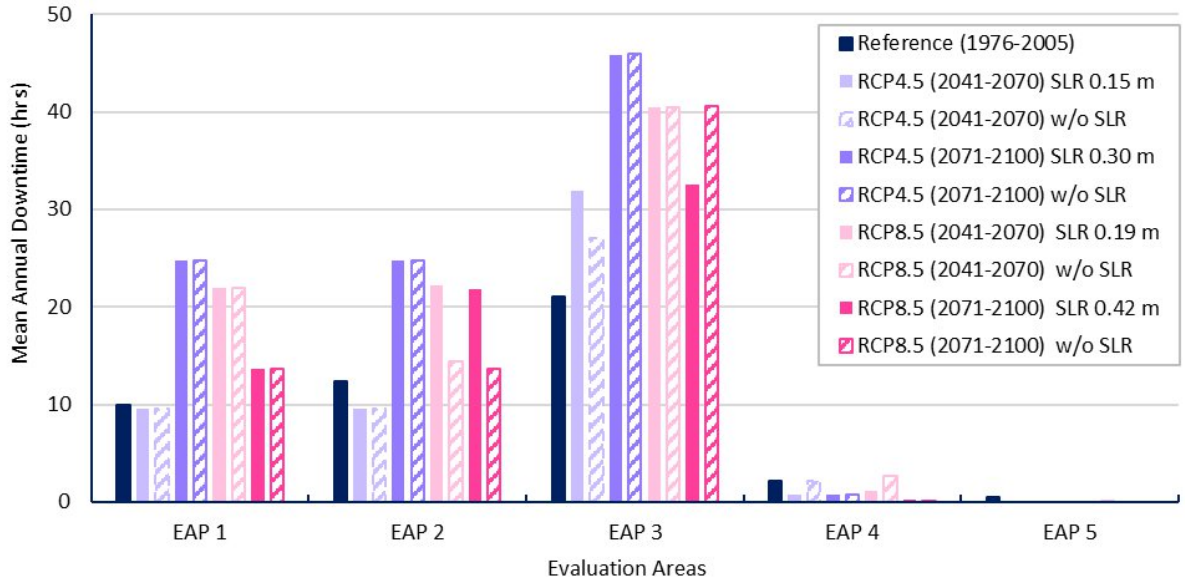

Fig. 17. Mean annual downtime per Evaluation Area and RCP scenario with and without (w/o) considering the SLR, for the Port of Piraeus.

3.2.2 Port of Limassol

An identical analysis was also conducted for the Port of Limassol. Figure 18 presents the simulation results for wave agitation, focusing on the largest waves recorded during each period and under each RCP scenario, originating from the direction with the highest frequency of occurrence (among those of interest), namely the East. It is observed that, as in the case of Piraeus, the largest wave (H_s = 4.45 m, T_p = 8.75 s) occurred in the dataset of the reference period (1976-2005). This wave generates the most significant disturbance within the port, impacting the entire basin, with wave heights reaching approximately 2 m. Overall, the Port of Limassol is also relatively well sheltered, though the berthing areas near the entrance (e.g., EAL2 and north of it) are more exposed. Extreme wave events from the east can lead to considerable agitation across the port basin, but these events occur with a low annual frequency.

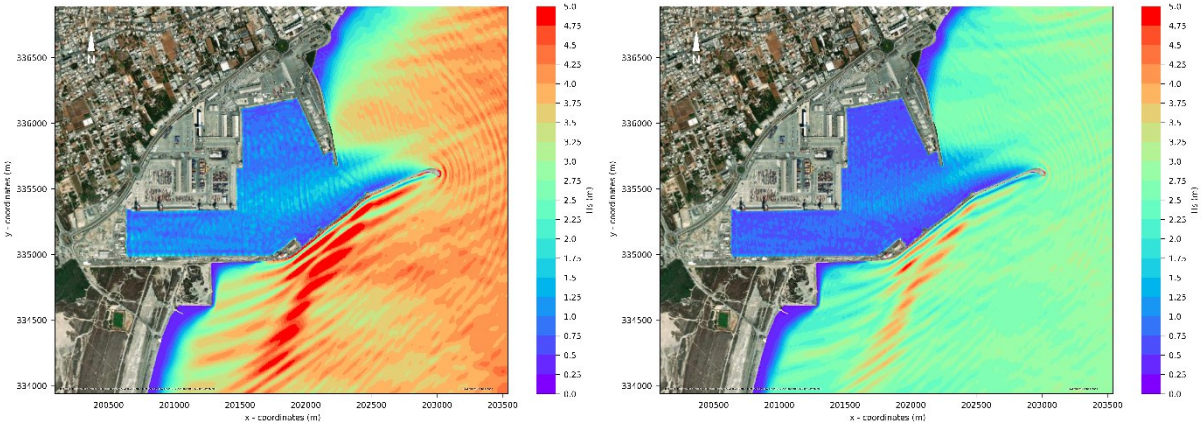

(a) Incident wave characteristics: H_s = 4.45 m, T_p = 8.75 s, MWD = 78 °; SLR = 0.00 m (Reference, 1976-2005).

(b) Incident wave characteristics: H_s = 3.14 m, T_p = 8.25 s, MWD = 79°, SLR = 0.48 m (RCP4.5, 2071-2100).

(c) Incident wave characteristics: H_s = 3.77 m, T_p = 9.05 s, MWD = 83°; SLR = 0.31 m (RCP8.5, 2041-2070).

(d) Incident wave characteristics: H_s = 3.05 m, T_p = 7.67 s, MWD = 81°; SLR = 0.62 m (RCP8.5, 2071-2100).

Fig. 18. Spatial distribution of wave heights for various individual incident wave scenarios, for the port of Limassol.

The results of the mean annual agitation are depicted in Figure 19 for the reference period (1976-2005), RCP4.5 (2041-2070, SLR = 0.27 m), RCP8.5 (2041-2070, SLR = 0.37 m), and RCP8.5 (2071-2100, SLR = 0.62 m). It is observed that offshore of the port, the mean annual agitation is relatively higher compared to any of the considered RCP scenarios. Within the port basin, a similar pattern is evident between the reference period and the RCP scenarios. However, a slight increase in the extent of agitation is noted for the RCP scenarios, particularly north of the EAL2. The same applies to RCP4.5 (2071-2100), although it is not shown here.

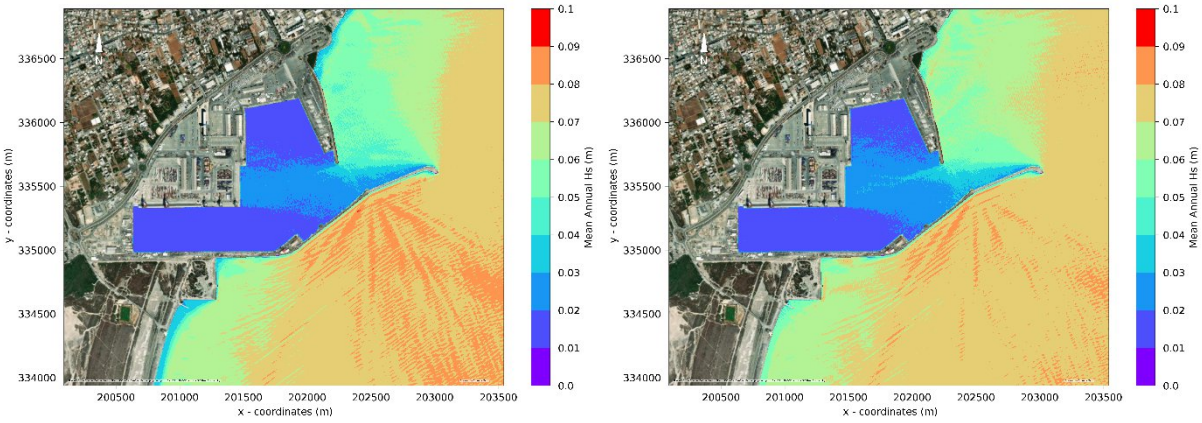

(a) Mean annual H_s for Reference data (1976-2005).

(b) Mean annual H_s for RCP4.5 (2041-2070, SLR = 0.27 m).

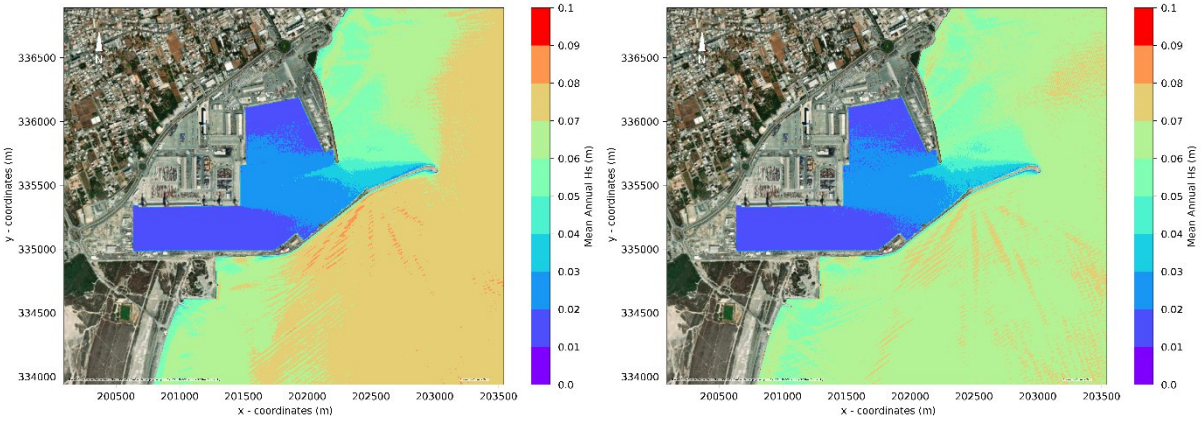

(c) Mean annual H_s for RCP8.5 (2041-2070, SLR = 0.37 m).

(d) Mean annual H_s for RCP8.5 (2071-2100, SLR = 0.62 m).

Fig. 19. Mean annual H_s for various scenarios, for the Port of Limassol.

Figure 20 presents the difference in mean annual agitation between the RCP scenarios and the Reference period. Within the port, there is no consistent trend of a uniform increase or decrease across all RCPs and periods examined. Significant deviations are not observed, with subareas showing both negative and positive differences. Notably, in the southwest basin, the differences are minimal, suggesting that this area is unlikely to be significantly impacted. Based on these results, it can be concluded that climate change will not necessarily lead to a uniform increase in wave agitation across all RCP scenarios – an observation consistent with the findings for the Port of Piraeus. Instead, the effects will vary depending on the specific RCP, the 30-year period, and the location within the port basin.

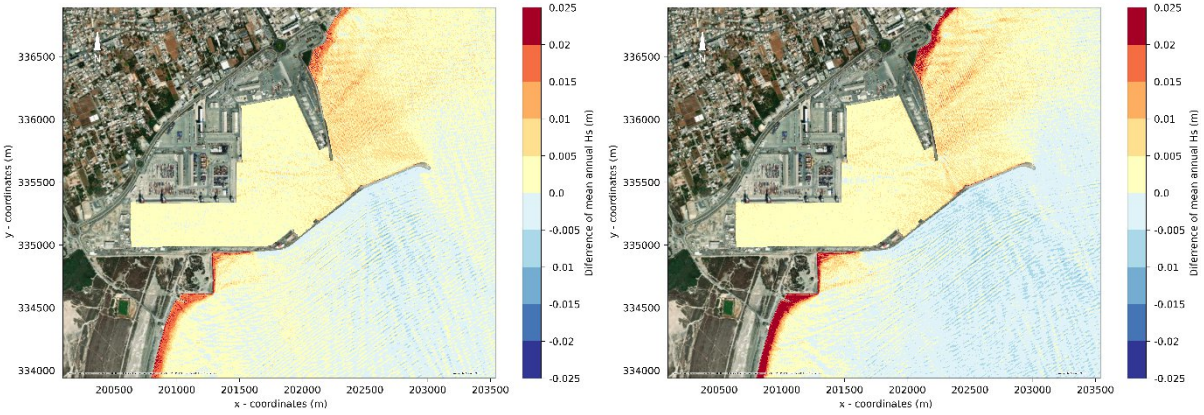

(a) Difference of mean annual H_s, between RCP4.5 (2041-2070, SLR = 0.27 m) and Reference period (1976-2005).

(b) Difference of mean annual H_s, between RCP4.5 (2071-2100, SLR = 0.48 m) and Reference period (1976-2005).

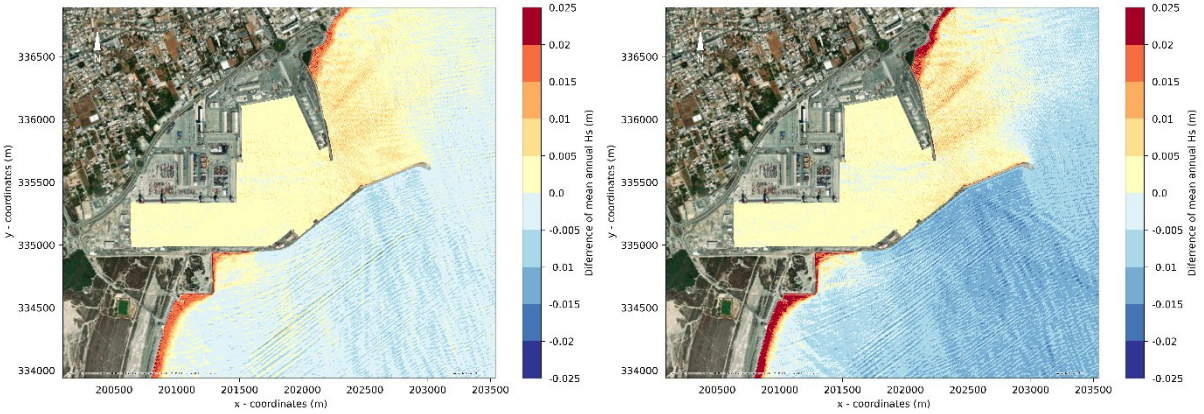

(c) Difference of mean annual H_s, between RCP8.5 (2041-2070, SLR = 0.31 m) and Reference period (1976-2005).

(d) Difference of mean annual H_s, between RCP8.5 (2071-2100, SLR = 0.62 m) and Reference period (1976-2005).

Fig. 20. Difference of mean annual H_s, between RCP scenarios and Reference period, for the Port of Limassol.

To clarify the impact of SLR on changes in mean annual wave agitation at the Port of Limassol, the differences between the RCP scenarios and the reference period were analyzed without accounting for SLR. As depicted in Fig. 21, no significant changes were observed, though the general trend suggests a slight reduction in wave agitation across all RCPs. For each RCP scenario, additional grids were created to represent the difference in mean annual agitation with and without considering SLR. As shown in Fig. 22, these differences remain at or above zero, indicating that SLR contributes to a modest increase in agitation, particularly at the port entrance and in the northern subbasin. These findings are consistent with those observed at the Port of Piraeus.

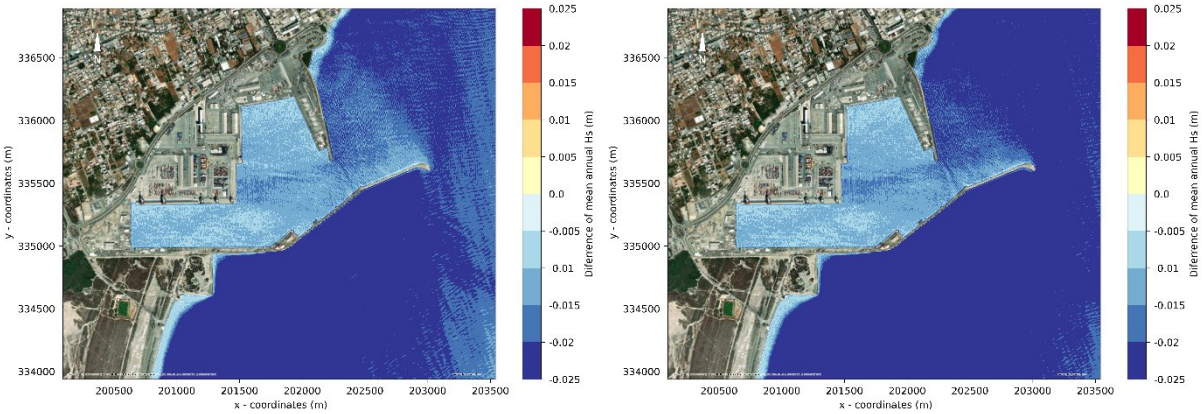

(a) Difference of mean annual H_s, between RCP4.5 (2041-2070, without SLR) and Reference period (1976-2005).

(b) Difference of mean annual H_s, between RCP4.5 (2071-2100, without SLR) and Reference period (1976-2005).

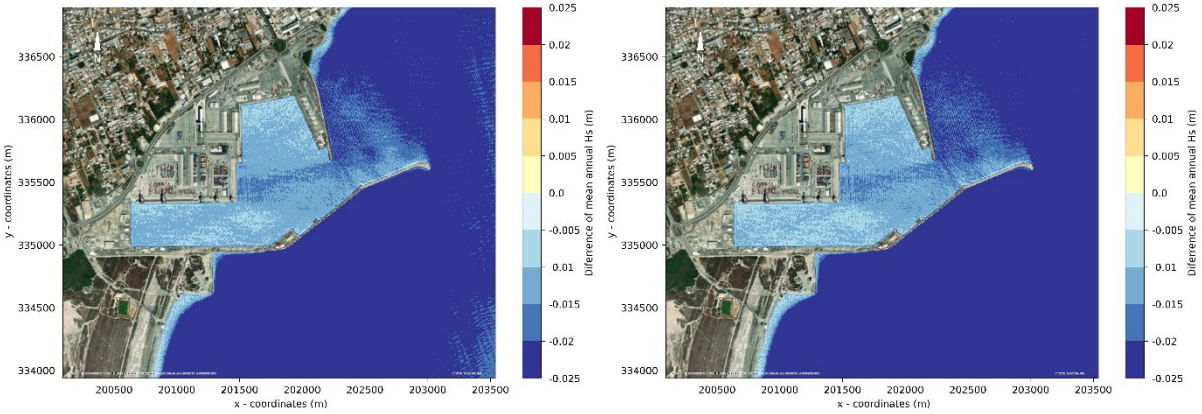

(c) Difference of mean annual H_s, between RCP8.5 (2041-2070, without SLR) and Reference period (1976-2005).

(d) Difference of mean annual H_s, between RCP8.5 (2071-2100, without SLR) and Reference period (1976-2005).

Fig. 21. Difference of mean annual H_s, between RCP scenarios, without considering SLR, and Reference period, for the Port of Limassol.

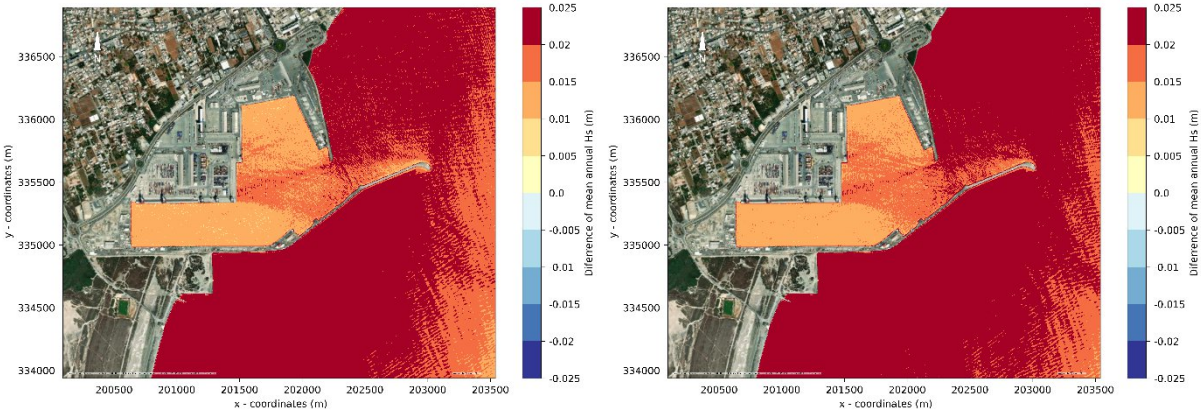

(a) Difference of mean annual H_s, for RCP4.5 (2041-2070), with and without considering SLR of 0.27 m.

(b) Difference of mean annual H_s, for RCP4.5 (2071-2100), with and without considering SLR of 0.48 m.

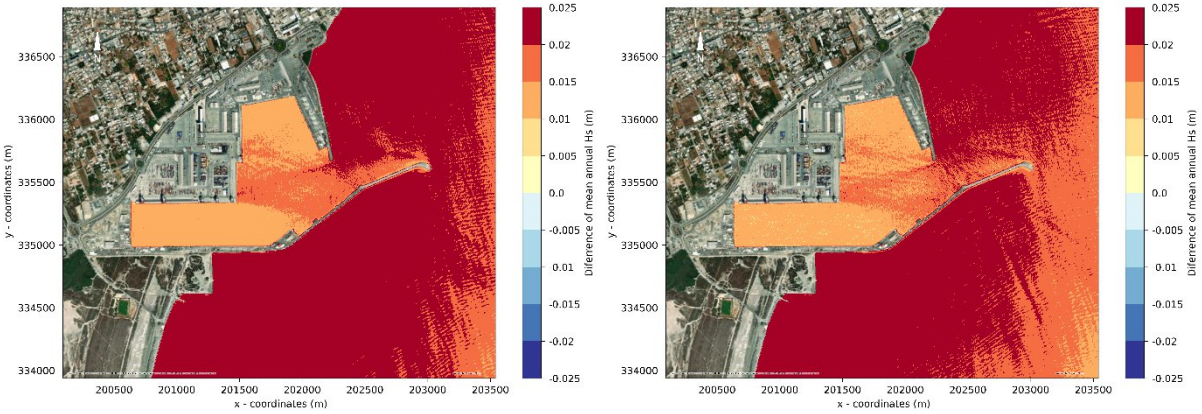

(c) Difference of mean annual H_s, for RCP8.5 (2041-2070), with and without considering SLR of 0.31 m.

(d) Difference of mean annual H_s, for RCP8.5 (2071-2100), with and without considering SLR of 0.62 m.

Fig. 22. Difference of mean annual H_s, for the investigated RCP scenarios, with and without considering the SLR, for the Port of Limassol.

The mean annual downtime for each EA, as defined in Figure 4, was also analyzed for all RCP scenarios and the hindcast period, both with and without considering SLR. Table 4 and Figure 23 present the resulting downtime. It is observed that the downtime for EAL1 remains relatively the same with the Reference period, across all RCP scenarios and periods, regardless of SLR's influence. For EAL2, a slight increase in downtime is observed only for the period 2041-2070, while for the period 2071-2100, the downtime remains nearly unchanged for both RCP scenarios. A notable increase is seen for EAL3, where downtime rises from 0.5 hrs during the reference period to a maximum of 7.1 hrs for the RCP4.5 scenario in 2071-2100. Similarly, an increase is noted for EAL4 and EAL5.

Regarding SLR's impact, no significant contribution was detected in most scenarios. In most cases, SLR had little effect on wave agitation. Nonetheless, in certain cases, incorporating SLR resulted in increased downtimes. For example, in EAL2 under the RCP4.5 scenario for the period 2071-2100, downtime increased from 5.2 hrs to 7.1 hrs when SLR was considered.

Table 4

Mean annual downtime (in hours) per Evaluation Area and RCP scenario with and without (w/o) considering the SLR, for the Port of Limassol.

Evaluation Areas	Reference (1976-2005)	RCP4.5 (2041-2070) SLR 0.15m	RCP4.5 (2041-2070) w/o SLR	RCP4.5 (2071-2100) SLR 0.30m	RCP4.5 (2071-2100) w/o SLR	RCP8.5 (2041-2070) SLR 0.19m	RCP8.5 (2041-2070) w/o SLR	RCP8.5 (2071-2100) SLR 0.42m	RCP8.5 (2071-2100) w/o SLR
EAL 1	15.1	16.8	16.6	15.9	15.9	17.8	17.8	15.5	15.5
EAL 2	62	71.4	71.4	61.8	60.2	69.6	69.6	62.1	59.6
EAL 3	0.5	4.7	4.7	7.1	5.2	1.8	1.6	6	6
EAL 4	0.3	0.2	1.8	1.2	1.2	1.6	1.6	1.5	1.5
EAL 5	0.2	0.2	1.8	0.3	0.3	1.6	1.6	1.5	1.5

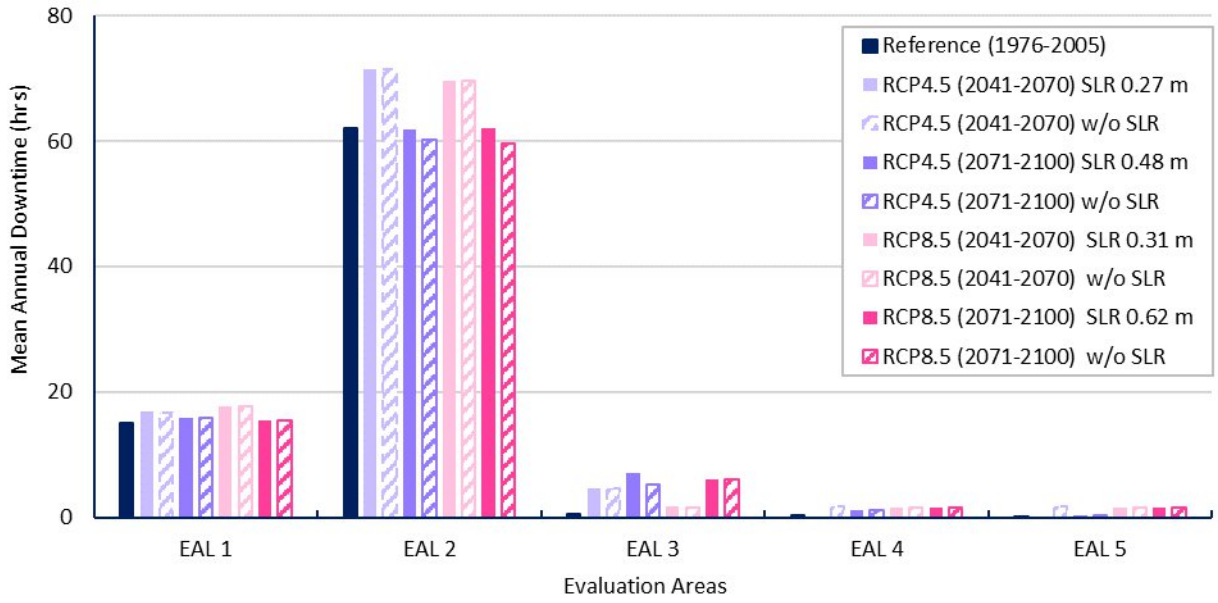

Fig. 23. Mean annual downtime per Evaluation Area and RCP scenario with and without (w/o) considering the SLR, for the Port of Limassol.

4 Conclusions

This study examined variations in mean annual wave agitation patterns and berth downtime for two key port basins in the eastern Mediterranean to inform their state of vulnerability—the passenger and cruise terminal of the Port of Piraeus in Greece and the Port of Limassol in Cyprus. The analysis was conducted under two climate scenarios (RCP4.5 and RCP8.5) up to 2100, using the reference period (1976-2005) for comparison. Changes in the offshore wave climate were assessed both with and without the influence of SLR to determine its specific impact on wave agitation. A high-fidelity

numerical model was employed to simulate wave agitation, capturing all dominant physical processes affecting both offshore areas and the port basins. The study focused on mean annual wave agitation across the entire basin and mean annual berth downtime at selected berthing locations.

With respect to the offshore wave climate, no substantial changes are detected for either port under both RCP scenarios during the analyzed periods, 2041–2070 and 2071–2100. However, a slight reduction in offshore mean annual wave agitation is observed at both ports compared to the reference period, primarily due to variations in mean annual wave heights and frequencies of occurrence. This reduction is more evident in the port of Piraeus compared to the port of Limassol.

Regarding the impact of climate change on mean annual wave agitation, no consistent pattern of increase or decrease is observed across the examined RCP scenarios and time periods for either port. For instance, in Piraeus under RCP4.5 (2071–2100), an increase in wave agitation is observed, whereas under RCP4.5 (2041–2070), a slight decrease is noted. Under RCP8.5, fluctuations occur, with both increases and decreases observed within the basin. These findings indicate that climate change will not result in a uniform increase in wave agitation, and outcomes will vary depending on the specific RCP, time period, and location within the port basin.

As for the influence of SLR in mean annual wave agitation, no significant changes are observed. However, the overall trend indicates a slight reduction in agitation across all RCPs when SLR is not considered, indicating that SLR contributes to an increase in agitation. This pattern is consistently observed at both ports.

For mean annual berth downtime, the more exposed sections in the outer basin of Piraeus (EAP1, EAP2, and EAP3) are projected to experience significant increases in downtime, particularly under the RCP4.5 (2071–2100) scenario, which appears to have the greatest impact. Interestingly, despite being the more extreme scenario, RCP8.5 does not necessarily result in the highest levels of average wave agitation, compared to RCP4.5. In Limassol, the most notable changes in mean annual berth downtime are expected in areas EAL3 to EAL5 (across both 30-year periods and under both RCP scenarios) and in EAL2 (specifically for the period 2041–2070), as these areas are more exposed.

With respect to the impact of SLR on mean annual berth downtime, no clear pattern emerges for the Port of Piraeus. Depending on the location, SLR may lead to an increase, decrease, or have no effect on downtime. In case of Limassol, no significant contribution of SLR to berth downtime was detected in most scenarios, with only minor increases in a few cases when SLR was considered.

In conclusion, wave agitation is a complex phenomenon influenced by a range of factors, including the incident sea state conditions, the geomorphology of the wider coastal area, the geometry and orientation of the port entrance, as well as the layout and characteristics of both outer protective structures and inner berthing works. The present study highlights that the projection of wave agitation

and resulting berth downtime is inherently case-specific, varying from port to port depending on local conditions and design features. Therefore, ports could undertake similar investigations to assess their future operability and potential exposure to increased downtime under changing climatic conditions. In this context, the implementation of continuous monitoring systems for wave agitation, alongside the development of forecasting tools, would provide valuable support in enhancing the resilience and operational planning of ports in the decades to come.

CRediT authorship contribution statement

Michalis Chondros: Conceptualization, Methodology, Software, Validation, Formal analysis, Investigation, Resources, Data Curation, Writing - Original Draft, Writing - Review & Editing, Visualization. **Andreas Papadimitriou**: Conceptualization, Methodology, Software, Validation, Formal analysis, Investigation, Resources, Data Curation, Writing - Original Draft, Writing - Review & Editing, Visualization. **Anastasios Metallinos**: Conceptualization, Methodology, Software, Validation, Formal analysis, Investigation, Resources, Data Curation, Writing - Original Draft, Writing - Review & Editing, Visualization. **Vasiliki Chalastani**: Investigation, Resources, Writing - Original Draft, Project administration, Funding acquisition. **Dimitris Spyrou**: Resources, Writing - Review & Editing, Funding acquisition. **Chrysi Laspidou**: Resources, Writing - Review & Editing, Supervision, Funding acquisition. **Phoebe Koundouri**: Resources, Writing - Review & Editing, Supervision, Funding acquisition. **Vasiliki Tsoukala**: Conceptualization, Methodology, Validation, Investigation, Resources, Writing - Review & Editing, Supervision, Project administration, Funding acquisition.

Declaration of competing interest

The authors declare that they have no known competing financial interests or personal relationships that could have appeared to influence the work reported in this paper.

Acknowledgements

The research described in this paper was conducted within the framework of the ARSINOE project, which has received funding from the European Union's HORIZON 2020 Innovation Action Programme under Grant Agreement No. 101037424.

The authors extend their appreciation to the authorities and operators of the Port of Piraeus and the Port of Limassol for sharing essential data.

References

Becker, A.H., Chase, N.T.L., Fischer, M., Schwegler, B., Mosher, K., 2016. A method to estimate climate-critical construction materials applied to seaport protection. Global Environmental Change 40:125–36. https://doi.org/10.1016/j.gloenvcha.2016.07.008.

Becker, A.H., Acciaro, M., Asariotis, R.*et al*.2013. A note on climate change adaptation for seaports: a challenge for global ports, a challenge for global society.*Climatic Change***120**, 683–695. https://doi.org/10.1007/s10584-013-0843-z

Caires, S., Yan, K., 2020. Ocean surface wave time series for the European coast from 1976 to 2100 derived from climate projections. Copernicus Climate Change Service (C3S) Climate Data Store (CDS). (Accessed on 21-02-2023), 10.24381/cds.572bf382.

Campos, A., García-Valdecasas, J. M., Molina, R., Castillo, C.,Álvarez-Fanjul, E., Staneva, J. 2019. Addressing long-term operational risk management in port docks under climate change scenarios. Water 11, 2153. https://doi.org/10.3390/w11102153

Camus, P., Tomás, A., Díaz-Hernández, G., Rodríguez, B., Izaguirre, C., Losada, I. J. 2019. Probabilistic assessment of port operation downtimes under climate change. Coast. Eng. 147, 12–24. https://doi.org/10.1016/j.coastaleng.2019.01.007

Casas-Prat, M., Sierra, J. P. 2010. Trend analysis of wave storminess: wave direction and its impact on harbour agitation. Nat. Hazard Earth Syst. Sci. 10, 2327– 2340. https://doi.org/10.5194/nhess-10-2327-2010

Chalastani, V.I.; Pantelidis, A.; Feloni, E.; Papadimitriou, A.; Tsaimou, C.N.; Nisiforou, O.; Tsoukala, V.K. 2023. Development of a Complex Vulnerability Index for Fishing Shelters—The Case of Cyprus.*J. Mar. Sci. Eng.11*, 1880. https://doi.org/10.3390/jmse11101880

Chengkun Li, Xiyi Yang, Dong Yang, 2025. Port vulnerability to natural disasters: An integrated view from hinterland to seaside, Transportation Research Part D: Transport and Environment, Volume 139, 104563, ISSN 1361-9209, https://doi.org/10.1016/j.trd.2024.104563

Chhetri, P., Corcoran, J., Gekara, V., Maddox, C., McEvoy, D., 2014. Seaport resilience to climate change: mapping vulnerability to sea-level rise.*Journal of Spatial Science*,*60*(1), 65–78. https://doi.org/10.1080/14498596.2014.943311

Chondros, M.K.; Metallinos, A.S.; Memos, C.D.; Karambas, T.V.; Papadimitriou, A.G. 2021. Concerted nonlinear mild-slope wave models for enhanced simulation of coastal processes. Appl. Math. Model. 91, 508–529. https://doi.org/10.1016/j.apm.2020.08.027

Chondros, M.K.; Metallinos, A.S.; Papadimitriou, A.G., 2024a. Enhanced Mild-Slope Wave Model with Parallel Implementation and Artificial Neural Network Support for Simulation of Wave Disturbance and Resonance in Ports. J. Mar. Sci. Eng. 2024, 12, 281. https://doi.org/10.3390/jmse12020281

Chondros, M.K.; Metallinos, A.S.; Papadimitriou, A.G., 2024b. Integrated Modeling of Coastal Processes Driven by an Advanced Mild Slope Wave Model. Modelling, 5, 458–482. https://doi.org/10.3390/modelling5020025

Church, J.A., P.U. Clark, A. Cazenave, J.M. Gregory, S. Jevrejeva, A. Levermann, M.A. Merrifield, G.A. Milne, R.S. Nerem, P.D. Nunn, A.J. Payne, W.T. Pfeffer, D. Stammer, A.S. Unnikrishnan, 2013: Sea Level Change. In: Climate Change 2013: The Physical Science Basis. Contribution of Working Group I to the Fifth Assessment Report of the Intergovernmental Panel on Climate Change [Stocker, T.F., D. Qin, G.-K. Plattner, M. Tignor, S.K. Allen, J. Boschung, A. Nauels, Y. Xia, V. Bex, P.M. Midgley (eds.)]. Cambridge University Press, Cambridge, United Kingdom and New York, NY, USA.

Cristina Izaguirre, Iñigo J. Losada, Paula Camus, Patricia González-Lamuño, Vladimir Stenek 2020. Seaport climate change impact assessment using a multi-level methodology, Maritime Policy & Management, 47:4, 544-557, https://doi.org/10.1080/03088839.2020.1725673

Fox-Kemper, B., H.T. Hewitt, C. Xiao, G. Aðalgeirsdóttir, S.S. Drijfhout, T.L. Edwards, N.R. Golledge, M. Hemer, R.E. Kopp, G. Krinner, A. Mix, D. Notz, S. Nowicki, I.S. Nurhati, L. Ruiz, J.-B. Sallée, A.B.A. Slangen, Y. Yu, 2021. Ocean, Cryosphere and Sea Level Change. In Climate Change 2021: The

Physical Science Basis. Contribution of Working Group I to the Sixth Assessment Report of the Intergovernmental Panel on Climate Change [Masson-Delmotte, V., P. Zhai, A. Pirani, S.L. Connors, C. Péan, S. Berger, N. Caud, Y. Chen, L. Goldfarb, M.I. Gomis, M. Huang, K. Leitzell, E. Lonnoy, J.B.R. Matthews, T.K. Maycock, T. Waterfield, O. Yelekçi, R. Yu, and B. Zhou (eds.)]. Cambridge University Press, Cambridge, United Kingdom and New York, NY, USA, pp. 1211–1362, https://doi.org/10.1017/9781009157896.011.

Garner, G. G., T. Hermans, R. E. Kopp, A. B. A. Slangen, T. L. Edwards, A. Levermann, S. Nowikci, M. D. Palmer, C. Smith, B. Fox-Kemper, H. T. Hewitt, C. Xiao, G. Aðalgeirsdóttir, S. S. Drijfhout, T. L. Edwards, N. R. Golledge, M. Hemer, G. Krinner, A. Mix, D. Notz, S. Nowicki, I. S. Nurhati, L. Ruiz, J-B. Sallée, Y. Yu, L. Hua, T. Palmer, B. Pearson, 2021. IPCC AR6 Sea Level Projections. Version 20210809. https://doi.org/10.5281/zenodo.5914709.

Hsieh, C. H., Tai, H. H., Lee, Y. N., 2013. Port vulnerability assessment from the perspective of critical infrastructure interdependency.*Maritime Policy & Management*,*41*(6), 589–606. https://doi.org/10.1080/03088839.2013.856523

IMO 2012.*International Shipping Facts and Figures—Information Resources on Trade*, *Safety*, *Security*, *Environment*; Maritime Knowledge Centre: London, UK.

Intergovernmental Panel on Climate Change, 2007. *Climate change 2007: Synthesis report. Contribution of Working Groups I, II and III to the Fourth Assessment Report of the Intergovernmental Panel on Climate Change* (Core Writing Team, R.K. Pachauri & A. Reisinger, Eds.). IPCC.

Izaguirre C., Losada I. J., Camus P., Vigh J. L., Stenek V., 2021. Climate change risk to global port operations.*Nat. Clim. Change*11, 14–20. https://doi.org/10.1038/s41558-020-00937-z

Kollias, I., Papadimitriou, A., Chondros, M., Chalastani, V., Spyrou, D., Laspidou, C., Koundouri, P., Tsoukala, V. 2023. Assessing the impact of Climate change in wave agitation for the port of Piraeus. E-Proceedings 2nd International Conference on Design and Management of Port, Coastal and Offshore Works, DMPCO, Thessaloniki, Greece, May 24-27 2023.

Kopp, R. E., Garner, G. G., Hermans, T. H. J., Jha, S., Kumar, P., Reedy, A., Slangen, A. B. A., Turilli, M., Edwards, T. L., Gregory, J. M., Koubbe, G., Levermann, A., Merzky, A., Nowicki, S., Palmer, M. D., Smith, C. 2023. The Framework for Assessing Changes To Sea-Level (FACTS) v1.0: A platform for characterizing parametric and structural uncertainty in future global, relative, and extreme sea-level change. Geoscientific Model Development, 16, 7461–7489. https://doi.org/10.5194/gmd-16-7461-2023.

McIntosh, R.D., Becker, A. 2020. Applying MCDA to weight indicators of seaport vulnerability to climate and extreme weather impacts for U.S. North Atlantic ports.*Environ Syst Decis***40**, 356–370. https://doi.org/10.1007/s10669-020-09767-y

Mohamed A. Abdelhafez, Bruce Ellingwood, Hussam Mahmoud. 2021 Vulnerability of seaports to hurricanes and sea level rise in a changing climate: A case study for mobile, AL, Coastal Engineering, Volume 167.

Ng, A.K.Y.; Zhang, H.; Afenyo, M.; Becker, A.; Cahoon, S.; Chen, S.-l.; Esteban, M.; Ferrari, C.; Lau, Y.-Y.; Lee, P.T.-W.; et al. 2018. Port Decision Maker Perceptions on the Effectiveness of Climate Adaptation Actions.*Coast. Manag. 46*, 148–175. https://doi.org/10.1080/08920753.2018.1451731

PIANC, 2014. Report No 121 – 2014, Harbour Approach Channels Design Guidelines

Puertos del Estado.1999.ROM 3.1-99: Recommendations for the Design of the Maritime Configuration of Ports, Approach Channels and Harbour Basins.Puertos del Estado, Madrid, Spain.

R. Duncan McIntosh, Austin Becker, 2019. Expert evaluation of open-data indicators of seaport vulnerability to climate and extreme weather impacts for U.S. North Atlantic ports, Ocean & Coastal Management, Volume 180, 104911, ISSN 0964-5691, https://doi.org/10.1016/j.ocecoaman.2019.104911

Scientia Maris, 2022: Maris HMS, User Guide, v02-2022, pp. 28.

Sierra JP, Sánchez-Arcilla A, Gironella X, Gracia V, Altomare C, Mösso C, Gonzá lez-Marco D, Gómez J, Barceló Mand Barahona, C., 2023. Impact of climate change on berthing areas in ports of the Balearic Islands: adaptation measures. Front. Mar. Sci. 10:1124763. https://doi.org/10.3389/fmars.2023.1124763

Sierra, J. P., Casas-Prat, M., Virgili, M., Mösso, C., Sánchez-Arcilla, A., 2015. Impacts on wave-driven harbour agitation due to climate change in Catalan ports. Nat. Hazard Earth Syst. Sci. 15, 1695–1709. https://doi.org/10.5194/nhess-15-1695-2015

Sierra, J. P., Genius, A., Lionello, P., Mestres, M., Mösso, C., Marzo, L., 2017. Modelling the impact of climate change on harbour operability: the Barcelona port case study. Ocean Eng. 141, 64–78. https://doi.org/10.1016/j.oceaneng.2017.06.002

UNCTAD, 2021.*Key Statistics and Trends in International Trade 2020*; UNCTAD: New York, NY, USA.

Winckler, P., Esparza, C., Mora, J., Melo, O., Bambach, N., Contreras-López, M., Sactic, M.I., 2022. Impacts in ports on a tectonically active coast for climate-driven projections under the RCP 8.5 scenario: 7 Chilean ports under scrutiny.*Coastal Engineering Journal*,*64*(3), 387–405. https://doi.org/10.1080/21664250.2022.2088194.

Zanuttigh, B.; van der Meer, J.W. 2008. Wave reflection from coastal structures in design conditions. Coast. Eng., 55, 771–779. https://doi.org/10.1016/j.coastaleng.2008.02.009.